MOLECULAR DYNAMICS SIMULATIONS OF HEAT TRANSFER IN NANOSCALE LIQUID FILMS

A Dissertation

by

BO HUNG KIM

Submitted to the Office of Graduate Studies of
Texas A&M University
in partial fulfillment of the requirements for the degree of

DOCTOR OF PHILOSOPHY

May 2009

Major Subject: Mechanical Engineering

MOLECULAR DYNAMICS SIMULATIONS OF HEAT TRANSFER IN NANOSCALE LIQUID FILMS

A Dissertation

by

BO HUNG KIM

Submitted to the Office of Graduate Studies of
Texas A&M University
in partial fulfillment of the requirements for the degree of

DOCTOR OF PHILOSOPHY

Approved by:

Co-Chairs of Committee,	Ali Beskok
	Tahir Cagin
Committee Members,	Debjyoti Banerjee
	Raymundo Arroyave
Head of Department,	Dennis O'Neal

May 2009

Major Subject: Mechanical Engineering

ABSTRACT

Molecular Dynamics Simulations of Heat Transfer

in Nanoscale Liquid Films. (May 2009)

Bo Hung Kim, B.A., Yonsei University;

M.S., Texas A&M University

Co-Chairs of Advisory Committee: Dr. Ali Beskok
Dr. Tahir Cagin

Molecular Dynamics (MD) simulations of nano-scale flows typically utilize fixed lattice crystal interactions between the fluid and stationary wall molecules. This approach cannot properly model thermal interactions at the wall-fluid interface. In order to properly simulate the flow and heat transfer in nano-scale channels, an interactive thermal wall model is developed. Using this model, the Fourier's law of heat conduction is verified in a 3.24 nm height channel, where linear temperature profiles with constant thermal conductivity is obtained. The thermal conductivity is verified using the predictions of Green-Kubo theory. MD simulations at different wall wettability ($\varepsilon_{wf}/\varepsilon$) and crystal bonding stiffness values (K) have shown temperature jumps at the liquid/solid interface, corresponding to the well known Kapitza resistance. Using systematic studies, the thermal resistance length at the interface is characterized as a function of the surface wettability, thermal oscillation frequency, wall temperature and thermal gradient. An empirical model for the thermal resistance length, which could be used as the jump-coefficient of a Navier boundary condition, is developed. Temperature

distributions in the nano-channels are predicted using analytical solution of the continuum heat conduction equation subjected to the new temperature jump condition, and validated using the MD results. Momentum and heat transfer in shear driven nano-channel flows are also investigated. Work done by the viscous stresses heats the fluid, which is dissipated through the channel walls, maintained at isothermal conditions. Spatial variations in the fluid density, kinematic viscosity, shear- and energy dissipation rates are presented. The energy dissipation rate is almost a constant for $\varepsilon_{\omega f}/\varepsilon < 0.6$, which results in parabolic temperature profiles in the domain with temperature jumps due to the Kapitza resistance at the liquid/solid interfaces. Using the energy dissipation rates predicted by MD simulations and the continuum energy equation subjected to the temperature jump boundary conditions developed in this study, the analytical solutions are obtained for the temperature profiles, which agree well with the MD results.

DEDICATION

For my grandmother

who lived a passionate life

through the age of turbulence

ACKNOWLEDGEMENTS

I would like to thank my committee co-chairs, Dr. Beskok and Dr. Cagin, and my committee members, Dr. Banerjee and Dr. Arroyave, for their guidance and support throughout the course of this research.

Also, thanks to my mother and father for their encouragement and to my wife for her patience and love.

TABLE OF CONTENTS

Page

LIST OF FIGURES

Page

Page

Page

LIST OF TABLES

CHAPTER I

INTRODUCTION*

In nano-scale flows, molecular structure of the fluid and surfaces, and their interactions between them at the atomistic length scales play a key role, and hence the molecular dynamics (MD) method emerges as a viable approach for investigation of the flow physics in such scales [1-3]. Recent developments in MD simulation of the nanoscale fluid flow are summarized in [4, 5]. As described in these two review articles, one of the primary interests in the nanoscale fluid flow is the investigation of fluid/surface interactions and their implication on the boundary conditions applicable for continuum level formulations. MD distinguishes itself from other simulation methods by providing atomistic level direct numerical experiments that enable simulations with various physical conditions. Therefore, MD can potentially address such issues as solid-fluid interfaces and interactions arising in the nanoscale-regime.

Previous nanoscale fluid flow MD simulations were focused on velocity slip on the boundary, and they have shown that the boundary slip on the liquid-solid interface is mainly a function of the wall-fluid interaction strength, fluid/wall density and shear rate [6, 7]. Many nanoscale fluid flow simulations had the fluid confined between two walls, and applied periodic boundary conditions in the flow direction. One of main objectives for this study is an implementation of physically sensible walls that realistically emulate solid-fluid interactions and thermal exchange between solid and the fluid. In most of the

---

This dissertation follows the style of *IEEE Transactions on Automatic Control.*

earlier simulations, a thermostat is applied to all fluid molecules in order to maintain the system at thermal equilibrium, and hence, the thermal boundary condition on the wall/fluid interface is often tampered by this choice.

In order to describe interactions of gas molecules with the surface, Maxwell [8] described specular and diffuse reflection models in 1897, which were appropriate in kinetic theory based approaches [9]. However, many MD simulations use more advanced wall models with fixed lattice structure instead of using simple specular walls. Fixed lattice walls consist of wall molecules fixed in their lattice positions and collide (interact) with fluid molecules via intermolecular forces [6, 10] without recoil. This model is similar to specular wall approach in terms of the energy conservation of the fluid confined within the wall boundary. However, it can facilitate application of a shear through the motion of the walls (i.e. changing the position of the wall molecules in every timestep). Similarly, instead of fixing the wall molecules in their lattice positions, it is possible to assign very heavy mass (e.g. $mass_{wall} = 10^{10} \times mass_{fluid}$) to wall molecules, which allows motion of wall molecules based on their interactions with fluid atoms and each other [11]. This enables the system to conserve its total energy, and prevents wall molecules from being swept away during the simulation. Since "fixed" lattice wall model impart energy to the system, it is necessary to utilize a thermostat to dissipate viscous heating induced by the shearing motion.

There are several widely accepted methods of applying thermostats to the model system in MD simulations to maintain the system's at constant temperature. To name a few, Anderson [12] developed a thermostat using stochastic forces that modify the

velocities to maintain average kinetic energy of the molecular system consistent with the equipartition theorem. Berendsen [13] developed a method that is efficient in relaxing the model system to a desired temperature by coupling an external bath at a constant temperature to the system and modifying the velocities at each iteration through a differential feedback mechanism. This efficient and widely used method though maintained constant temperature thermodynamics state, does not produce canonical probability distribution in momentum space during simulations [2]. The most popular thermostat that sustains the canonical ensemble distribution both in configuration and momentum space is the Nose-Hoover thermostat, which generates canonical temperature fluctuations by affecting intermolecular forces from extended ensemble system. It was first suggested by Nose [14, 15], and then modified by Hoover [16].

Although, thermostats in the system can be used to maintain isothermal state of the system in equilibrium MD simulations, care should be taken when they are used in steady state simulations where thermal transport and fluid flow is critical. Notably, physically sound approaches should be implemented to model the thermal transport at the wall-fluid interfaces. Sun *et al*. [17] utilized a 'diffuse reflection' model, which accounted the interactions between the fluid and wall molecules through the use of mathematically smooth walls that reflect fluid molecules with random thermal velocities based on the Maxwell-Boltzmann velocity distribution. However, with the authors' candid admission this model could only be a crude approximation of real physics at the wall/fluid interface. In order to improve their model, Sun *et al*. developed an advanced 'diffuse reflection' wall model [18], which reflected both fluid and wall molecules with

random thermal velocities. Although, this model enabled energy transfer between the wall and fluid, it presented difficulties in implementations of moving boundaries.

A more advanced wall model utilizes a lattice of molecules connected to crystal positions with harmonic bonding. Ceiplak *et al.,* [19] examined boundary conditions at the wall-fluid interface using harmonic springs attached to the lattice position of each wall molecule, which allowed the wall molecules to vibrate, emulating the thermal motion of solid crystals. In order to confine the displacements of the oscillating wall molecules, the authors used high stiffness constants for bonding [19]. Though this represents a remarkable advance to model the wall lattice fluid interactions, a thermostat was deemed necessary to maintain the fluid temperature in equilibrium [19, 20]. Thermal equilibrium state of the fluid was readily and uniformly maintained through the application of thermostat, which dissipated heat due to viscous heating to the imaginary heat reservoir, instead of through the collision/interaction with the neighboring walls. Hence, the thermal interactions between the fluid and surfaces which may have distance dependence through the fluid system were not modeled adequately.

In order to properly consider the nature of thermal transport at the wall-fluid interface, the lattice wall model with a characteristic bonding stiffness was used. Thermal oscillations of wall molecules influence the fluid by absorbing or supplying momentum and energy to fluid molecules via intermolecular interactions. Walls are utilized as heat baths to maintain thermal equilibrium of the fluid, therefore there was no need to apply a thermostat uniformly to the equations of motion for the fluid molecules to maintain the system at constant temperature during simulations. Thermal ‘natural’

interactions between the fluid and wall maintained the thermal equilibrium of the fluid, while the temperature of the wall was kept constant. In the case of shear driven flow, energy imparted on the fluid (i.e., work done by the moving wall) was dissipated by the fluid as viscous heating, while constant wall temperature applied on the surface enabled heat loss through the walls.

CHAPTER II

INTERACTIVE THERMAL WALLS*

Previous MD simulations of nano-confined liquid flows have shown "velocity slip" at the liquid/solid interface, depending on the interaction strength (wettability) of liquid and solid molecules (see Chapters 10-13 in [1] and the references therein). In order to investigate boundary slip in fluid-wall interface, Two-dimensional MD simulations were performed for shear driven flow in a 5 nm width channel. For interatomic interactions, the most commonly used and simple interaction potential (Lennard-Jones 12-6 potential) was employed. The form of Lennard-Jones 12-6 potential is $V(r_{ij}) = 4\varepsilon\left[\left(\frac{\sigma}{r_{ij}}\right)^{12} - \left(\frac{\sigma}{r_{ij}}\right)^{6}\right]$, where ε is the binding energy (depth of the potential) and σ is the molecular diameter (the distance at which the interparticle potential is 0). The first term represents the short range repulsive interactions preventing the overlap of the molecules, while the second term represents a dipole-induced attractive interaction. The interaction force is between a pair is given by $F_{ij}(r_{ij}) = -\frac{\partial V(r_{ij})}{\partial r_{ij}}$. The temperature of the simulation was set to 120K, and the number density (N/σ^2) of the system is ρ=0.8, which corresponded to the liquid state of argon [10]. The temperature in a 2-dimensional N particle system can be defined through the average kinetic energy as $\left\langle \sum_i \frac{m_i v_i^2}{2} \right\rangle = \frac{dNkT}{2}$. For argon molecule molecular mass is m= 6.69×10^{-26} kg, molecular diameter is σ = 0.34

*Reprinted with permission from "Thermal interactions in nanoscale fluid flow: molecular dynamics simulations with solid–liquid interfaces" by B. H. Kim., A. Beskok., T. Cagin., *Microfluidics and Nanofluidics*, Volume 5, Pages 551-559, Copyright 2008 by Springer.

nm and binding energy ε is 119.8×k_b (1.6539×10^{-21} J). Intermolecular interaction forces were truncated to zero at a cut-off distance of 1.0nm, which is approximately at 3σ. The top and bottom surfaces were moved in opposite directions with the speed of $U_w = 0.5\sqrt{\varepsilon/m}$ as shown in Fig. 1.

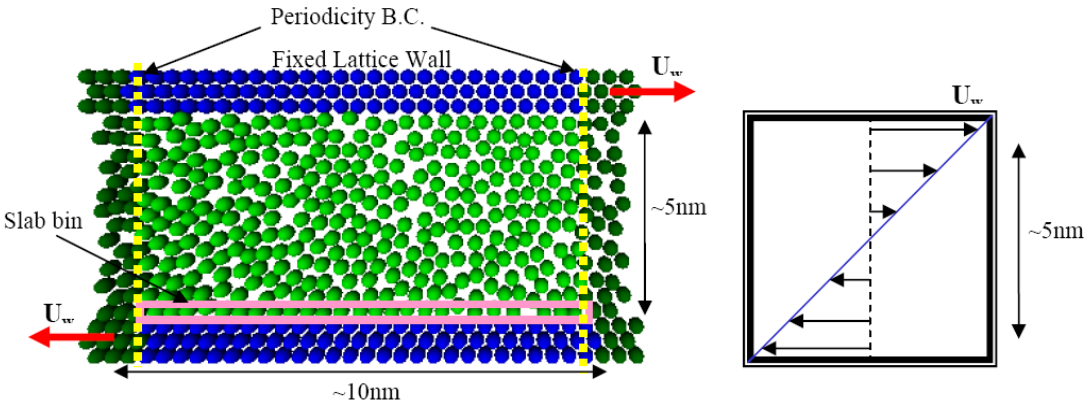

Figure 1. Schematics of shear driven flow in a 5nm wide channel. Model contained 313 fluid molecules with fixed lattice crystal walls at moving at a shear rate $\dot{\gamma} = 3.14\times10^{10}\text{s}^{-1}$. Shaded molecules outside the box in periodic boundary directions are the images of fluid mapped using periodic boundary condition over the domain of interaction.

Characteristic time $\tau = \sigma\sqrt{m/\varepsilon}$ is 2.16×10^{-12} s, and the simulations used 4fs (~0.002τ) time steps. Periodicity boundary conditions were imposed in the streamwise direction as described in [21]. For computational simplicity two-dimensional MD simulations were performed. A total of 313 fluid molecules (N_f = 313) were simulated in

a 2D 5nm width channel. For establishing the baseline for the approach and testing the developed code, the fixed lattice wall model was applied first. Since the walls were modeled as perfectly elastic fixed lattice crystals, there is no heat transfer to/from the walls [10]. Under such unrealistic thermal interface model, the temperature of the system steadily increases if any kind of work is done on the system. Therefore, it is necessary to dissipate work done by the moving wall using a thermostat (Nose-Hoover). In this thermalized wall model, the temperature of the fluid is maintained around 120 K, as desired. However, thermal transport at the fluid-wall interface has no physical meaning.

Before presenting simulation results with new simulation set up, which utilize the interactive thermal wall model, it is important to reproduce and compare the results at similar conditions with previous MD simulations that utilized fixed lattice crystal walls. Fig. 2 shows comparisons of the velocity profiles obtained from the MD simulations and the results in [10] for fluid and wall interaction potential strengths of ε_{wf}= 0.4ε, 1ε and 4. The simulations started from Maxwell-Boltzmann velocity distribution, and ran 1.2×10^6 time-steps (4.8ns) to reach the steady state, after which, another 1.2×10^6 timesteps were performed for time averaging. Longer time averaging has also been performed to confirm convergence of local velocity and temperature to steady state. The computations with the fixed lattice crystal wall cases are presented only for code verification purposes, where the fluid temperature is maintained a constant using Nose-Hoover thermostat [22]. The velocity profiles obtained from fixed lattice wall cases match the results in [10], which predict the same velocity-stick and velocity-slip behavior.

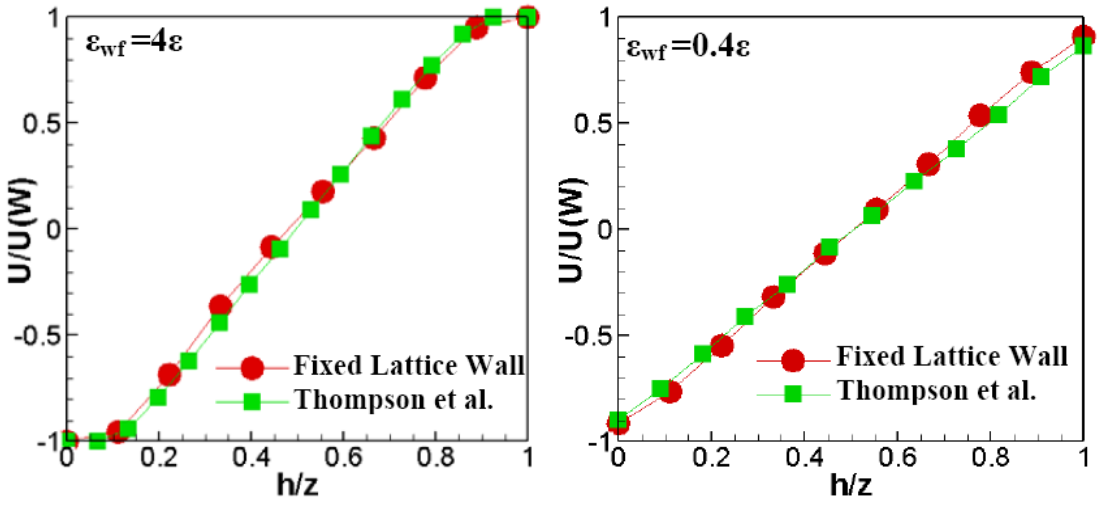

Figure 2. Velocity slip/stick on the walls at various liquid/wall interaction strengths. Comparison is made with the results obtained by Thompson *et al.* in [10].

Prior to the presentation of the temperature profiles, it is important to demonstrate local thermal equilibrium in the system. Local temperature can be defined only if local thermal equilibrium is established. Using MD simulations with stochastic thermal walls and by applying a thermal gradient, Tenenbaum calculated density and temperature profiles in a nano channel, and demonstrated local thermal equilibrium by comparisons with the predictions of an equation of state [23]. Another methodology for verification of local thermal equilibrium is calculation of the higher moments of velocity. At equilibrium, the velocity distribution at the point of measure should have normal (Gaussian) distribution with zero skewness and kurtosis. For *all cases* presented in this

chapter, higher moments of the velocity distribution is calculated for the first slab bin adjacent to the bottom wall and for a bin at the channel center. The results have shown almost normal distribution of the velocity with skewness and kurtosis varying between -0.097 to 0.054 and -0.092 to 0.202, respectively. Therefore local thermal equilibrium in the fluid was maintained for all of MD simulations. For steady results, the ensemble was collected at every 5^{th} time-step for 25,000 time-steps (100ps) to obtain a reasonable ensemble average. For the transient (freezing) case, shorter collection time (5000 time-steps - 20ps) was used to present temperature distribution at 20ps intervals. As a result, kurtosis of the transient case was slightly larger (-0.092 to 0.202) than the steady state cases (0.012 to 0.023).

Thermal Walls Interacting with Fluid Molecules

In order to properly implement thermal interactions between the fluid and wall molecules, lattice bond springs were utilized as described in [19, 20], which were attached to the wall molecules at their lattice positions. Moreover, more advanced thermal interaction mechanisms were included to the walls. For initial conditions, the velocities for thermal oscillations were assigned from a Maxwell-Boltzmann distribution consistent with the target temperature, and then the thermostat was applied to wall molecules to absorb/supply heat from/to the fluid via wall/fluid interactions.

Previous nanoscale MD simulations defined important features of the boundary slip on nanoscale fluid flows as function of the strength of wall/fluid interactions, the density of fluid and the shear rate. However, their results did not properly include

thermal interactions between wall and fluid. In order to improve this, newly developed interactive thermal wall model has its own thermal oscillations and it exchanges momentum and energy between fluid and the wall. Therefore, excessive heat in the fluid is transferred to the walls, and then, the heat is dissipated through the thermostat applied on the walls.

The velocity Verlet algorithm was used for time integration [21]. In order to find the position and velocity of molecules at the next time step, evaluation of intermolecular forces are required. Detailed forces of interactions experienced by each of the fluid molecule and wall molecules are calculated separately by using interaction potentials between fluid molecules and fluid molecules and wall molecules. The total force experienced by a fluid molecule is therefore a sum of these two terms:

$$F_{fluid}(r_i) = \sum_{j=1}^{N_f} \frac{\partial V(r_{ij})_{fluid-fluid}}{\partial r_{ij}} + \sum_{j=1}^{N_w} \frac{\partial V(r_{ij})_{fluid-wall}}{\partial r_{ij}}. \quad (1)$$

Every fluid molecule interacts with other fluid or wall molecules within the predetermined cutoff distance. The forces depend on interparticle distances. Hence, thermal oscillations of wall molecules affect the forces acting on the fluid molecules through this variation of their position as well. In order to properly implement the thermal interactions between fluid and wall molecules properly, the forces due to fluid molecules on the motion of wall molecules must be taken into account while reducing the interactions between molecules of wall to a crystal bond-stiffness and defining each as independent oscillators. The resulting force on a molecule of the wall is given as

$$F_{wall}(r_i) = \sum_{j=1}^{N_f} \frac{\partial V(r_{ij})_{wall-fluid}}{\partial r_{ij}} + K(|r_0 - r_i|), \quad (2)$$

where K is the wall crystal bonding stiffness and $|r_0\text{-}r_i|$ is the distance between the original lattice position and current position of the wall molecule. Equation (1) is the force exerted on a fluid molecule by the surrounding fluid and wall molecules, while equation (2) is the force exerted on a wall molecule by fluid molecules and the attached lattice springs. The ideal way of constructing a wall as a heat reservoir is to form thermally oscillating crystals with an infinite number of molecules, and then make those wall molecules interact with each other. However, including interactions between very large numbers of wall molecules are computationally prohibitive. Moreover, the main focus was not on the thermal behavior of solid walls but the proper characterization of thermal interactions of fluid molecules with the wall. Therefore, it is most efficient to construct interactive thermal walls without including the N_w^2 interactions between the wall molecules while maintaining physics.

For the interactive thermal wall model, velocity scaling thermostat is applied to each wall layer separately with parameter $\eta_{layer} = \sqrt{\frac{T_{assigned-wall}}{T_{layer-wall}}}$ at every time step. Since there were no interactions between the crystal layers, these scaling surrogate the thermal interactions between the layers of lattice wall crystals, and keeps all layers at a prescribed temperature. For initial conditions, interactive thermal walls have thermal oscillations described by the Boltzmann velocity distribution at a desired temperature. As the simulation proceeds, thermal oscillations of wall molecules are affected from

wall/fluid interactions, which enable heat transfer from fluid to the wall. Since wall molecules do not interact with each other, cut off distance of 1nm is enough for the thickness of the wall modeled using three layers of wall molecules, and the thermostat should be applied to each layer of the lattice crystal molecules separately, as shown in Fig 3. Otherwise, the 1st layer (surface) of the wall, which adjoins to the fluid, would have most of the thermal velocity distribution, and a relatively high temperature as compared to the average wall temperature. In comparison to the ideal "all atom-all interacting" wall case that requires additional N_w^2 operations to properly exchange heat with the fluid, the interactive thermal wall model is computationally cheap, and yet it is as effective as the ideal wall model. Moreover, by applying thermostats to each layer of the wall, there is no omission of thermal interactions between fluid/wall molecules. Therefore, viscous heating is dissipated thorough the isothermal walls.

Shear driven nano-flow simulations with same configuration to that in Fig. 2 are repeated using the new interactive thermal wall model utilizing crystal bonding stiffness of $K = 64\left(4\varepsilon/\sigma^2\right)$. The velocity profiles obtained from the new thermal model are compared with the fixed lattice wall model in Fig. 4. Velocity profiles predicted by both models are similar to each other. However, there are significant differences between the two models in the prediction of temperature profile. Work done by the shearing of walls induces viscous heating to the fluid, while the system reaches to steady state by heat dissipation through the walls. As a result, temperature distribution in the fluid shows parabolic profiles with a jump at the wall/fluid interface (Fig. 5). Parabolic temperature distribution is expected, since the shear rate is a constant in the entire domain, which not

only results in a linear velocity profile, but also a constant heating rate. Surprisingly this behavior is observationally similar to that of rarefied gas flow in shear-driven micro-channel, which exhibits a linear velocity profile with slip, and a parabolic temperature distribution with jumps [2]. Despite these similarities, physical reasons for these jumps are different between gas and liquid flows.

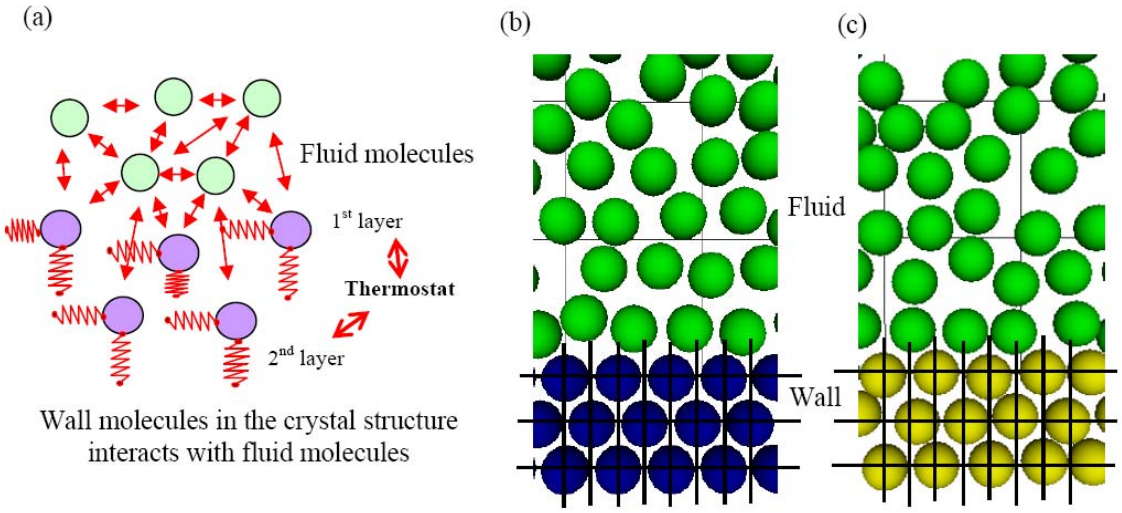

Figure 3. (a) Schematics representation of thermal wall-fluid interactions using a crystal bond spring attaches the molecules to their lattice positions; (b) Wall molecules fixed in a lattice position; (c) A snapshot of the wall molecules in thermal oscillations (deviated from their lattice position) interacting with fluid molecules.

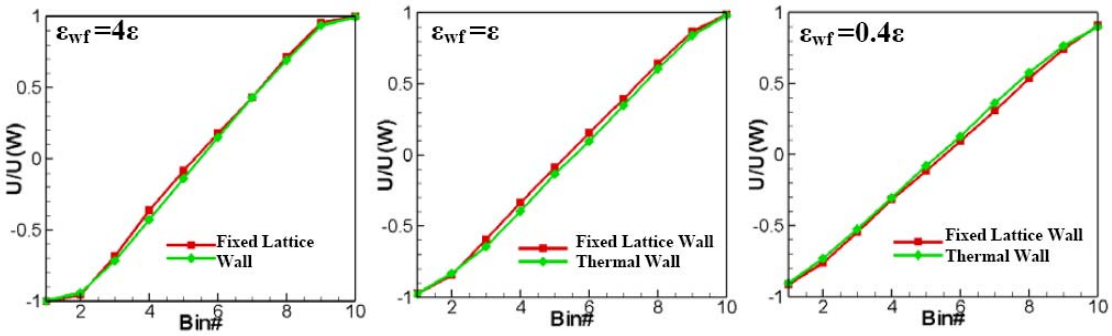

Figure 4. Velocity profiles resulted in shear-driven flow simulations with interactive thermal wall model and fixed lattice crystal walls.

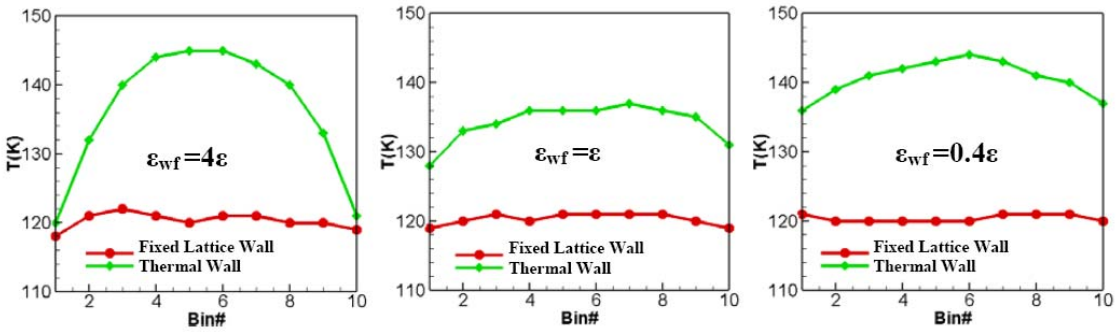

Figure 5. Temperature profiles resulted in simulations with fixed lattice crystal wall model and with the interactive thermal wall model at various wall/fluid interaction strengths.

Different thermal oscillation frequencies of two dissimilar materials induce a thermal resistance at their interface. Thermal resistance of metal/liquid-helium interface was first discovered by Kapitza (1941), and it is also known as the Kapitza resistance [24]. The classical theory to explain heat transfer between solid/liquid interfaces

basically assumes the thermal resistance on the interface to essentially depend on the phonon density, which determines the heat transmission ratio between the two dissimilar materials [25]. However a recent MD study has shown that surface wettability (i.e., wall/fluid interaction strength) also enhanced the heat transmission ratio on the solid/liquid interface [26]. Fig. 5 shows how the wall/fluid interaction strength (surface wettability) in the shear flow affects the interface temperature jump while it causes velocity locking or slip of the fluid. Moreover, for strong attractive walls, MD studies have shown layering effects of the liquid molecules next to the surface and the layered structure went through a transition as the interaction strength changes [27], and the structural changes of the layered molecules also changes thermal conductance at the interface [28].

Results in Fig. 5 show temperature jump being a function of the wall/fluid interaction strength, which results in different thermal (Kapitza) resistance on the interface. Strong interactive forces reduce both the temperature jumps and velocity slip at the interface. However, the fixed lattice model, which applies the Nose-Hoover thermostat on the fluid, shows almost uniform temperature distribution. Therefore, thermal interactions between the fluid and wall predicted by the fixed lattice wall model are unphysical. In order to investigate further for the effects of thermal oscillation frequency, heat transfer MD simulations with two different crystal bonding stiffness are presented in the next section.

Temperature Jumps on High Crystal Bond Stiffness

Previously, Thompson *et al.,* have investigated velocity slip on the boundary as functions of the wall/fluid interaction potential strength, wall density and shear rate [6, 7]. As shown in the previous section, the interactive thermal wall shows similar velocity slip results with the fixed lattice wall model. However, the temperature profiles inside the channel are significantly different. Moreover, a temperature jump is observed at the boundary when the wall/fluid interaction potential is weak. The temperature jump at the boundary is caused by fluid molecules near the wall boundary that have different thermal velocity from the wall. Since the local temperature of a system defined through the thermal velocities of molecules, effective momentum transfer between the wall and fluid is important. If the wall/fluid interactions are weaker or less effective than the fluid/fluid interactions, it is obvious that the thermal motions of fluid molecules are more dominantly influenced by the neighboring molecules of fluid rather than the neighboring wall molecules. Therefore, weak wall/fluid interactions generate a momentum deficit at the wall/fluid interface. This causes sudden changes in distribution of local kinetic energy, which is directly related to the temperature jump at the interface. Therefore, it is obvious that, when there are strong wall/fluid molecular interactions, there is no temperature jump as shown in Fig. 5. (a). Density also plays an important role because the more dense the system is, there is more opportunity for the interactions between the wall and fluid molecules.

Crystal bonding stiffness constant, K, is an additional parameter for the wall/fluid interface that has an affect on the temperature jump. For a simple harmonic oscillating

system with constant total energy, stiffness of the system determines the oscillation frequency, the amplitude is mainly determined by the temperature of wall (but the anharmonicity induced by the interactions between wall and fluid molecules becomes more dominant if K is soft, hence larger amplitude motion may result). Since the temperature is measured through time averaged kinetic energy, different bond stiffness generates different kinetic energy fluctuations; still the averages of the kinetic energy are the same. Therefore, for walls at the same temperature, larger crystal bonding stiffness generates higher frequency thermal oscillations with smaller deviations from the temperature dictated amplitudes.

In order to investigate further the relation between the temperature jump and the crystal bonding stiffness, two nanoscale heat transfer MD simulations were performed by using different bonding stiffness constants, K in equation (2). Two different crystal bonding stiffness constants K_1 and K_2 are determined from the second derivative of the Lennard-Jones potential for wall molecules for the distance where pairwise energy is minimum. This corresponds to the curvature of the potential well; Here K_2 is five times larger than K_1. The distance between the walls is taken as 10nm, $\varepsilon_{wf}=\varepsilon$ and number density is $\rho=0.8$. Temperature at the bottom and top walls are 80K and 160K, respectively. Fig 6 shows that the temperature jump was observed at large stiffness ($K_2 = 320\left(4\varepsilon/\sigma^2\right)$) values, However, at $K_1 = 64\left(4\varepsilon/\sigma^2\right)$, compliant with the thermal oscillation of fluid molecules at density $\rho=0.8$, there was no temperature jump. This shows the importance of the crystal bonding stiffness K for thermal equilibrium at the liquid/solid interface. Thermal equilibrium at the interface also depends on the

effectiveness of momentum transfer between the wall and fluid molecules and their impact on thermal oscillations of the molecules of walls. Figures 5 and 6 show that at low fluid densities, weak wall/fluid interaction potential as well as large crystal bonding stiffness provide less effective momentum transfer between the wall and liquid molecules, and results in larger Kapitza resistance. Increased Kapitza resistance on the interface shows deviation in the local kinetic energy distribution and results in temperature jumps at the wall/liquid interface.

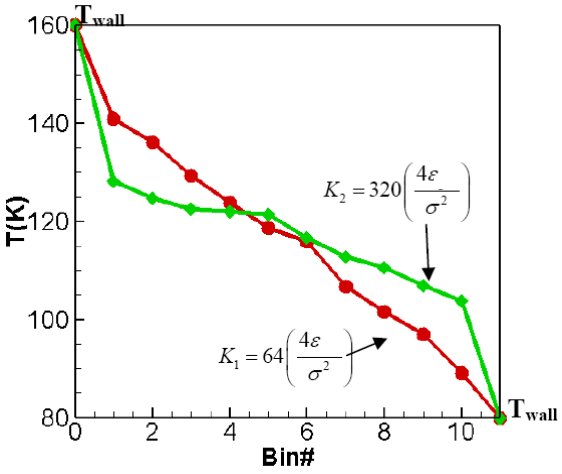

Figure 6. Temperature profile dependence (over the 10 slabs -each with 1 nm thickness, channel width 10nm) on different crystal bonding stiffness values ($K_2 = 5\ K_1$).

Transient Heat Transfer Simulations

In this section, MD simulation results for a transient heat transfer problem are presented. Initially, the simulation domain has a 10nm distance between the walls, and

the temperature for interactive thermal walls ($K_1 = 64\left(4\varepsilon/\sigma^2\right)$, $\varepsilon_{wf} = \varepsilon$) and argon fluid molecules (ρ=0.8) was set to 200K. Periodic boundary condition was applied in the streamwise direction. From the equilibrium state at 200K, the wall temperature was suddenly dropped to 20K using the thermostats. Naturally, the wall started absorbing heat from the liquid. Due to heat transfer through the wall, thermal motions of liquid molecules are slow down as they moved to lower energy states in configuration space as well. Hence, the liquid molecules near the wall started to crystallize (freeze) as shown in Fig. 7 (a). Fig. 7 (b) shows the number density fluctuation of fluid molecules in each of the slab bins between the walls. Each slab bin has a width of 0.1 nm and a length of 10 nm. This density fluctuation (ρ_{bin}-ρ_{avg}) shows layering of fluid molecules as it crystallizes. Moreover, the figure enables us to observe the process of crystallization. At earlier times, the liquid region shows limited density fluctuations along the width of the channel, because the molecules can freely move in the liquid state. However, in the case of crystallized molecules, the number density fluctuates across the channel as shown at 400 to 420ps time frames in Fig. 7 (b).

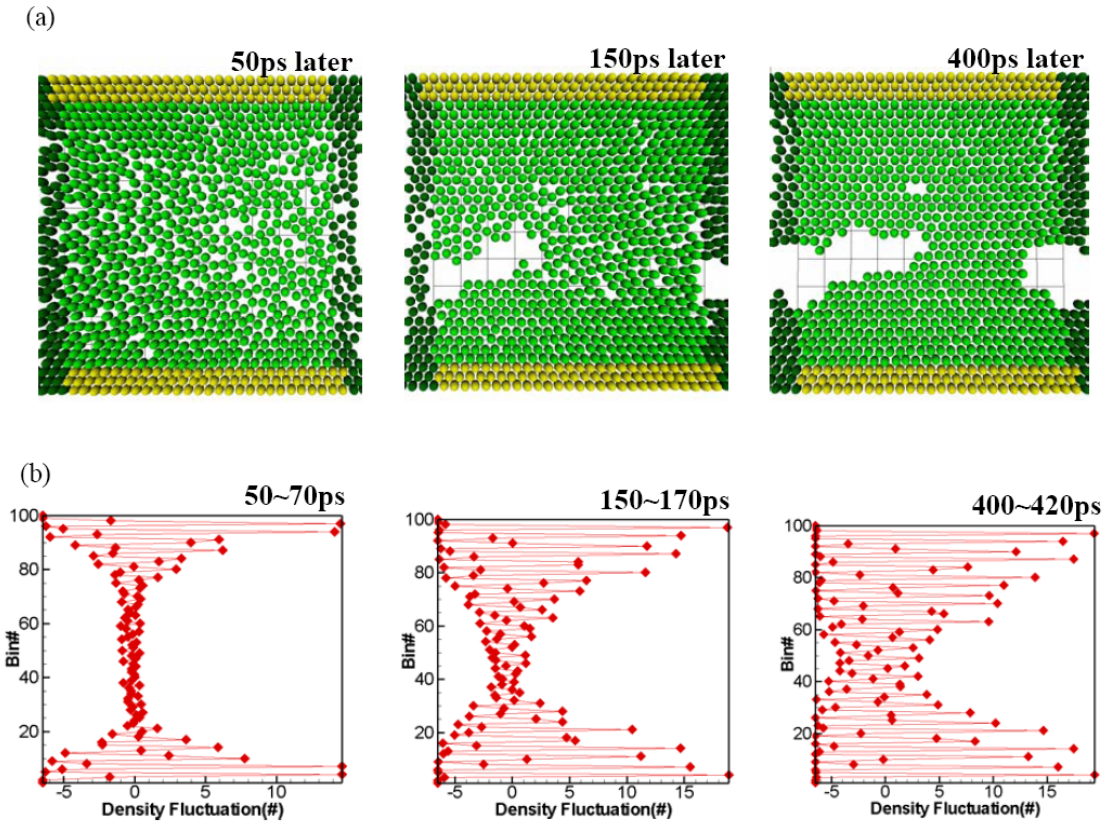

Figure 7. Freezing process of argon, initially at 200K and in contact with two walls at 20K (a). Density fluctuations (ρ_{bin}-ρ_{avg}) in 0.1×10nm slab bins as a function of time (b).

Fig 8 shows the transient local temperature of the initially hot (200K) liquid between two cold (at T=20K) walls during the cooling process. Each of the temperature profile was averaged for 20ps to smooth out the statistical fluctuations. The liquid temperature reaches the equilibrium state temperature of 20K after 400ps. However, temperature of the wall and fluid are different at the beginning of the cooling process, even though the wall ($\varepsilon_{wf}=\varepsilon$) had compliant crystal bonding stiffness (K_1). This result is

significantly different than the continuum theory that predicts the same temperature at the interface.

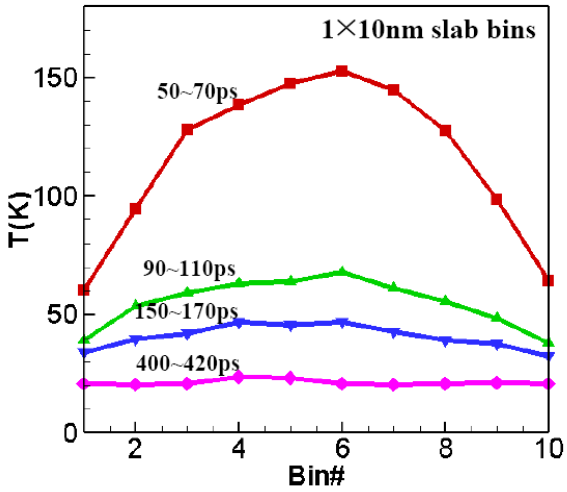

Figure 8. Temperature distribution at various times for the freezing process shown in figure 7.

CHAPTER III

INTERFACE THERMAL RESISTANCE*

Recent developments in nano-science and technology instigated vast number of investigations of mass, momentum and energy transport in nano-scale structures, and flow conduits [2]. Most theoretical investigations utilize the molecular dynamics (MD) method, which enables proper resolution of the molecular structure of fluid and surfaces, and models their interactions at atomic length and time scales. Despite the extensive research on nano-scale fluid flow and velocity-slip at the liquid/solid interface, heat transport in nano-scale flow conduits have not been investigated in great detail. This lack of information is not only due to the difficulty of experimenting in nano-scales, but also due to the limitations of typical MD method in handling thermal interactions of molecules with walls. In the previous chapter, a new interactive thermal wall model was developed and it allowed us to simulate flow and heat transfer in two-dimensional nano-channels. The new thermal model predicted "velocity slip" at the liquid/solid interface equally well with the results published in the literature. It has also shown "temperature-jumps" at the interface, both for shear-driven nano-scale flows and for a transient phase-change process.

Thermal transport through an interface between two dissimilar materials is known to result in a temperature jump (ΔT_i). For a given or measured heat flux ($\vec{j}$), this jump can be identified as a thermal resistance (R_K), written as

$$\Delta T_i = -R_K \vec{j} \cdot \vec{n} \,, \tag{3}$$

*Reprinted with permission from "Molecular dynamics simulations of thermal resistance at the liquid-solid interface" by B. H. Kim., A. Beskok., T. Cagin., Journal of Chemical Physics, Volume 129, Page 174701, Copyright 2008 by American Institute of Physics.

where and $\vec{n}$ is the outward unit normal from the wall. This interface resistance was discovered by Kapitza in 1941 on a metal-liquid interface [24], and hence, known as the Kapitza resistance. Similar to the velocity slip-length, one can define a thermal resistance length (L_K, known as the Kapitza length), by extrapolating the temperature profile from liquid in to the solid, where wall temperature is reached (Fig. 9). The Kapitza length can be predicted as

$$\Delta T_i = L_K \left.\frac{\partial T}{\partial n}\right|_{liquid}, \tag{4}$$

where $\partial T/\partial n$ is the thermal gradient on the liquid side, and $\Delta T_i = T_{fluid} - T_{wall}$. Being able to define a thermal gradient requires onset of continuum approximation, where the temperature and its gradient can be defined. If Fourier's law ($\vec{j} = -\lambda \nabla T$) is valid with constant thermal conductivity (λ), then equations (3) and (4) can be related as $L_K = R_K \lambda$. Under such conditions, Kapitza length is the equivalent thickness of liquid with the same thermal conductivity that causes equivalent thermal resistance on the interface. Furthermore, equation (4) can be utilized as a boundary condition at the liquid/solid interface. Overall, equations (3) and (4) along with the Fourier's law are based on the continuum approximation, which may not be applicable to nano-scale fluidic systems. However, proper coverage of the field requires a summary of previous studies, including the continuum based models.

(a)

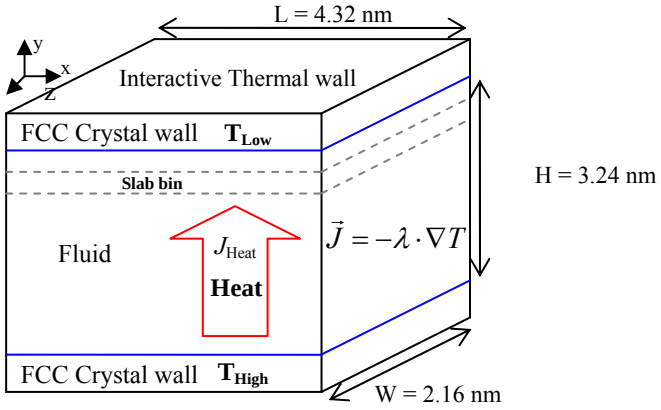

(b)

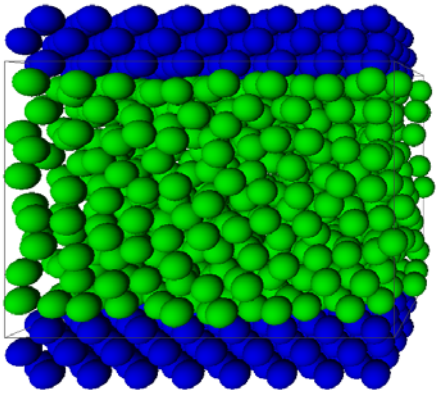

(c)

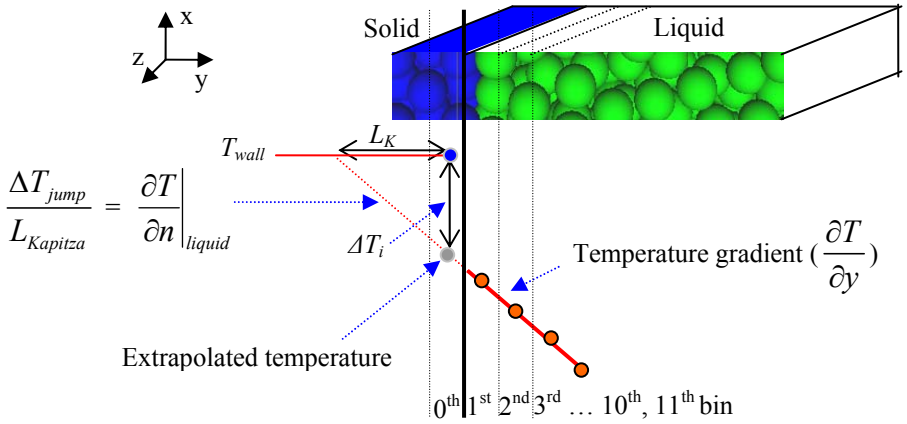

Figure 9. (a) Schematics of MD simulation of steady state heat transfer. (b) A snapshot of fluid and wall molecules. (c) Definitions of bins, wall location, temperature jump and Kapitza length.

The Acoustic Mismatch Model (AMM) explains thermal resistance at the liquid/solid interface as a function of the phonon density, which determines the heat transmission ratio between the two dissimilar materials [25]. AMM defines a transmission probability between the liquid/solid interface. It provides a simplified theory based on continuum acoustics, which treats phonons as plane waves that could be transmitted or reflected at the interface [29]. A simple description of the acoustic mismatch model is that each medium can be described with an acoustic impedance of $Z_i=\rho_i c_i$, which is the product between the density ρ and phonon velocity c of medium i. The acoustic mismatch model defines the heat transmission probability τ as

$$\tau_{1\to 2}=\frac{4Z_2Z_1}{\left(Z_1+Z_2\right)^2}, \tag{5}$$

where the interface thermal resistance R_K is a function of $1/\tau$ [30]. In AMM, R_K depends on the thermal oscillation frequency, which is related with the effective intermolecular stiffness (c_i^2 is proportional to the effective intermolecular stiffness K_i [31]). Predictions of AMM are only applicable to extremely low temperatures and exhibits large deviations at room temperature. Other continuum based theories, such as the Scattering Mediated Acoustic Mismatch Model (SMAMM) had been developed from AMM, which included more information about the microscopic principles such as phonon scattering or radiative heat transfer [32]. However, SMAMM still employed simplified assumptions of the molecular structure and their interactions, which are critical in nano-scale heat transfer. Swartz *et al.* [29] developed the Diffuse Mismatch Model (DMM) to supplement AMM. In DMM, the phonon scattering at an interface affected the heat transmission coefficient

proportional to the phonon density. These classical theories utilized simplified characteristics of the molecular structure and molecular interactions, and they were not able to fully explain the complexities of thermal resistance at the interface of two dissimilar materials [30].

Several limitations of the continuum-based models can be overcome using MD. For example, the surface wettability (i.e., liquid/solid interaction strength) was not considered either in AMM or DMM. Using MD, strong wetting of a solid surface was shown to enhance thermal transport to the liquid, and exponentially decrease L_K [31]. Heat transmission ratio on the interface was also enhanced [26]. Another MD study investigated thermal conductance at the interface as a function of the liquid/solid interaction strength, where strong interactions resulted in layering of fluid molecules on solid surfaces [27]. In addition, structural changes of the layered molecules were reported to alter thermal conductance at the interface [28]. For monatomic molecules, this layered molecular structure did not affect the thermal interface significantly. However, complex liquids like polymers or polar fluids like water might form thicker layers or characteristic structures which may significantly affect the thermal resistance on the interface [33]. In, [34]predictions of MD simulations which included details of the nano-scale structure and molecular interactions were compared with the predictions of DMM theory. Based on these findings, MD simulations were utilized to examine the temperature dependence of the interface thermal resistance [35]. Previous investigations have shown the importance of molecular level structure and interaction on heat transfer at the liquid/solid interface, which produced large deviations from the classical theories.

However, there has been no comprehensive MD-derived thermal resistance model, which can substitute or extend the classical theories.

In this chapter, three-dimensional heat conduction between parallel plates separated by a thin layer of liquid argon was investigated. Developed 3D-MD algorithm utilizes the interactive thermal wall model presented and verified in the previous chapter, which enables efficient computational modeling of thermal transport between two isothermal surfaces. The *objectives* of this chapter are as follows: First, validation of Fourier's law in a nano-channel, and verify thermal conductivity using the Green-Kubo theory. Then characterize the empirical-model and verify the thermal resistance length (L_K) at the interface as a function of the surface wettability, thermal oscillation frequency, wall temperature, thermal gradients and channel height.

Validity of Fourier's Law

In order to check the validity of Fourier's law in nano-scale regime and investigate the interface thermal resistance, it is necessary to calculate the heat flux, thermal conductivity of the liquid, and the temperature distribution. Generally, two methods can be applied for thermal conductivity calculations in MD simulations [36]. One approach is the Green-Kubo method that is based on the fluctuation-dissipation theorem, and applicable for the equilibrium MD technique. The Green-Kubo method is derived from the linear response theory to extract thermal conductivity from the energy current correlation function. The second approach is the utilization of Fourier's law, which is based on a linear constitutive law, and may not be applicable in nano-confined geometries. Both methods require heat flux ($\vec{j}$), calculated from the net energy of every

molecule in the system.

First, thermal conductivity of liquid argon using the Green-Kubo method was calculated. When there are no electronic contributions and net flow in the system, thermal motion becomes the sole contributor in calculation of thermal conductivity [37]. In order to calculate the heat current, the energy equation is utilized as

$$\frac{1}{\Omega}\frac{\partial h(\vec{r},t)}{\partial t}+\nabla\cdot\vec{j}\left(\vec{r},t\right)=0\,, \tag{6}$$

where Ω is volume of the system, h_i is the total energy of molecule i, which includes kinetic ($\frac{p_i^2}{2m_i}$) and potential (V) energies. P_i is the momentum ($m_i v_i$), m_i is the mass and v_i is the velocity of molecule i. For pairwise interactions,

$$h_i=\frac{p_i^2}{2m_i}+\frac{1}{2}\sum_j V_{ij}\,. \tag{7}$$

Therefore,

$$\vec{j}(t)=\frac{1}{\Omega}\frac{d}{dt}\sum_i \vec{r}_i h_i\,, \tag{8}$$

and

$$\vec{j}(t)=\frac{1}{\Omega}\left[\sum_{i=1}^{N}\left(v_i h_i+\frac{1}{2}\sum_{j=1,j\neq i}^{N} r_{ij}(F_{ij}\cdot v_i)\right)\right], \tag{9}$$

where the F_{ij} is the force acting on molecule i from the molecule j. Using the fluctuation-dissipation theorem, thermal conductivity for an isotropic system is expressed in terms of the heat current correlation function as

$$\lambda=\frac{1}{3\Omega k_B T^2}\int_0^\infty\left\langle\vec{J}(0)\vec{J}(t)\right\rangle dt\,. \tag{10}$$

This equation is numerically discretized as

$$\lambda = \frac{\Delta t}{3\Omega k_B T^2} \sum_{m=1}^{M} \frac{1}{(N-M)} \sum_{n=1}^{N-m} \vec{J}(m+n) \cdot \vec{J}(n), \tag{11}$$

where $\vec{J}$ is $\vec{j} \times \Omega$, T is the system temperature, M is the averaging timestep and N is the number of simulation timesteps for calculation of the actual heat vector correlation. N should be large enough to assure convergence of the heat vector correlation function, and M must be large enough for averaging but it should be much less than N [36]. In MD simulations, N was set as 1×10^6 for the heat vector correlation function calculation, and M as 5×10^4 for the averaging step. For the equilibrium state of the *NVT* ensemble, Nose-Hoover thermostat [22] was applied to the molecules to maintain the system's temperature at 100K, and the number density ($N\sigma^{3/}\Omega$) of the system was set at ρ~0.8. The Lennard-Jones potential $V(r_{ij}) = 4\varepsilon\left[\left(\frac{\sigma}{r_{ij}}\right)^{12} - \left(\frac{\sigma}{r_{ij}}\right)^{6}\right]$ was utilized and the mass for an argon molecule was m= 6.63×10^{-26} kg, the molecular diameter was σ = 0.3405 nm and the depth of the potential well (ε) for argon is $119.8\times k_b$ (1.6539×10^{-21} J). Intermolecular interaction forces were truncated and switched to zero at a cut-off distance of 1.08 nm, which is approximately at 3σ. The velocity Verlet algorithm was used for time integration [21] and characteristic time $\tau = \sigma\sqrt{m/\varepsilon}$ is 2.16×10^{-12} s, and the simulations used 4 fs (~0.002τ) timesteps. 550 molecules used in a periodic box which is large enough for calculation of bulk thermal conductivity of argon [38]. The 3D-MD code successfully calculated the thermal conductivity of liquid argon using Green Kubo

method as presented in Table 1, which includes comparisons with published values in the literature.

Table 1**.** Thermal conductivity of liquid argon at 100K obtained using the Fourier's law and Green-Kubo method.

Averaged heat current of the liquid between 90K and 110K walls	Thermal conductivity using Fourier's Law	Thermal conductivity using Green-Kubo method	Borgelt et al. at 102.3K [39]	McGaughey et al. at 100K [40]
4.63×10^{8} W/m^2	101.24 *m*W/mK	103.2 *m*W/mK	102.7 *m*W/mK	110 *m*W/mK

In order to test the validity of Fourier's law of heat conduction in a nano-scale channel, A thermal gradient was induced in the fluid using two different constant temperature walls (90K and 110K) on the top and bottom channel surfaces. A total of 578 fluid molecules were simulated in a 3D channel of height (*H*) 3.24 nm, and width (*W*) 2.16 nm and length (*L*) of 4.32 nm. The number density ($N\sigma^{3/}\Omega$) of the system was $\rho\sim0.8$, which corresponded to the liquid state of argon around 100K. Fig. 9 shows the schematics and dimensions of the simulation domain that has the interactive thermal walls with perfect FCC crystal (001) surfaces. Periodic boundary conditions are imposed in x and z directions. Temperature distribution in the fluid is obtained using 10 slab bins (numbered as 1~10) parallel to the walls. The 0^{th} and 11^{th} bins represent the bottom and top walls, respectively. As shown in Fig. 9 (c), the 1^{st} and 10^{th} bins start at the centerline of wall molecules. Hence, these bins partially contain wall molecules at certain times. Overall, the bin width is smaller than the molecular diameter, and both liquid and wall

molecules are in thermal motion. Thus definition of the wall boundary may be indistinct. For this purpose, walls were defined at the 0^{th} and 11^{th} bins, and measured the Kapitza length using linear extrapolation of the temperature profile till the desired wall temperature (T_{wall}) is achieved. In definition of the temperature jump, extrapolated temperatures were utilized at the 0^{th} and 11^{th} bins. Using the similar triangles rule, it is possible to show that the Kapitza length (L_K) defined by the convention can have a maximum deviation of $\sigma/2$, if the walls were defined at the interfaces of the 0^{th} and 1^{st}, and 10^{th} and 11^{th} bins, respectively. Such a change in convention brings about 0.17 nm variation in the predictions of L_K.

Temperature distribution of liquid argon between 90K and 110K walls is shown in Fig. 10. Linear temperature variation in the channel enables us to test the validity of Fourier's law, given as

$$\vec{j} = -\lambda \cdot \nabla T, \tag{12}$$

where $\vec{j}$ is the steady state heat flux produced by the temperature gradient ∇T. The heat flux was calculated using equation (9). Having the temperature gradient from MD simulations, one can estimate the thermal conductivity (λ) using Fourier's law. Comparison of thermal conductivity obtained from the Green-Kubo method with that extracted from the Fourier's law of heat conduction enables assessment of reliability of Fourier's law in nano confined dimensions.

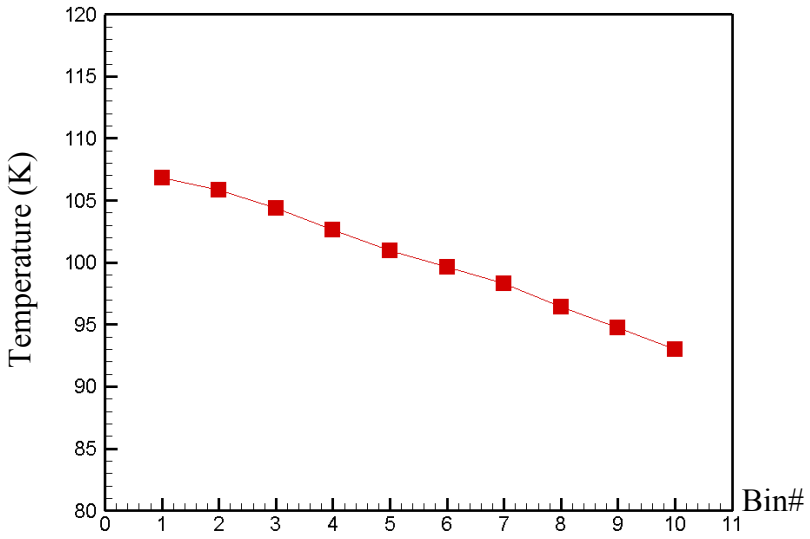

Figure 10. Temperature variation of liquid argon in 10 slab bins along the channel height. Top and bottom walls are kept at 90K and 110K, respectively.

In order to minimize the influence of interface thermal resistance due to the acoustic mismatch, the crystal bonding stiffness is chose as $K=K_w$, where $K_w = 64\left(4\varepsilon/\sigma^2\right)$ corresponds to the effective intermolecular stiffness of liquid argon, calculated from the compliant part of the curvature of the potential well based on the 12-6 Lennard-Jones potential. The interaction strength between liquid/solid and iquid/liquid is chosen to be the same ($\varepsilon_{wf}=\varepsilon$). $K=K_w$ produces thermal oscillations of wall molecules similar to that of the fluid molecules. However, $K=K_w$ is stiff enough to prevent melting of the solid crystal walls. Simulations started from the Maxwell-Boltzmann velocity distribution both for liquid and walls, and ran 2×10^5 time-steps (0.8ns) to reach a steady state, after which another 4×10^5 timesteps (1.6ns) were performed for time averaging. Longer time

averaging has also been performed to confirm convergence of heat flux and temperature profiles to the steady state. Time averaged temperature profile between the top wall and bottom walls shown in Fig. 10 exhibits a linear variation, typical of continuum predictions. Thermal conductivity of liquid argon was obtained using the Fourier's law using equation (4) with heat flux and a time averaged temperature gradient predicted from MD. Thermal conductivity calculated from Fourier's law is 0.101 W/mK as shown in Table 1. This value matches well with the previously published thermal conductivity of liquid argon around 100K, which was shown to be 0.09 ~ 0.12 W/mK with a 7~10% error range [38-40]. Considering the amount of heat flux (4.63×10^{8} W/m^2) and the size of the simulation domain ($\Omega = 30.23\times10^{-27}$ m^3), MD simulations successfully reproduce the thermal conductivity of liquid argon using Fourier's law.

Temperature Jump on the Interface and Kapitza Length

The classical theories such as AMM and DMM mainly assume that the thermal resistance on the interface is induced by the acoustic mismatch between two dissimilar materials [25, 29]. However, recent MD studies have shown that the surface wettability (i.e. interaction strength) also plays an important role in the interface thermal resistance. In order to quantify the thermal resistance of the interface, the *Kapitza resistance* R_K [26] was utilized as defined in equation (3). When Fourier's law is valid, equation (4) relates the Kapitza length with R_K, since $\frac{\Delta T_i}{L_K} = \left.\frac{\partial T}{\partial n}\right|_{liquid}$ and $L_K = R_K \lambda$ as shown in Fig. 9. In order to develop a comprehensive model for predicting the temperature jump at the interface (ΔT_i), hypothesizing that the temperature jump is a function of the relative

thermal oscillation frequency of wall and liquid (ω_w/ω_f), liquid/solid interaction strength ($\varepsilon_{wf}/\varepsilon$, i.e., surface wettability), wall Temperature (T_w) and the local thermal gradient ($\partial T/\partial n$). Note that utilization of the thermal gradient requires definition of a length scale. Therefore, systematic simulations were performed by varying nano-channel dimensions. Overall, $\Delta T_i = f(\frac{\omega_w}{\omega_f}, \frac{\varepsilon_{wf}}{\varepsilon}, T_w, \frac{\partial T}{\partial n})$ was assumed that the parameters are consistent with the key findings in the literature.

Effect of Thermal Oscillation Frequency

In order to investigate the influence of different thermal oscillations on the interface thermal resistance, crystal bonding stiffness K of lattice crystal walls were changed where the thermal oscillation frequency is approximately predicted as $\omega \approx \sqrt{K/m}$. The crystal bonding stiffness K for each simulation is assigned differently. K=K_w was chosen for the point of reference, where $K_w = 64\left(4\varepsilon/\sigma^2\right)$, and varied K from K_w to $9K_w$. The interaction strength between liquid/solid and liquid/liquid is set equal (ε_{wf} =ε). Temperature difference between the bottom and top walls is increased to 70K to obtain larger temperature jumps, and to reduce thermal noise. The bottom wall was set to 160K and the top wall was set to 90K. Fig. 11 shows the temperature profiles and temperature gradient changes in liquid argon for different crystal bonding stiffness values. Essentially linear temperature variations are reported in the fluid, with temperature jumps increasing with increased crystal bonding stiffness. The temperature profiles shown in Fig. 11 (top) do not cross each other exactly at the same point between

the 5th and 6th bins, since the temperature jump is also a function of the wall temperature. Bottom figure shows the temperature gradient, which decreases with increased K_w.

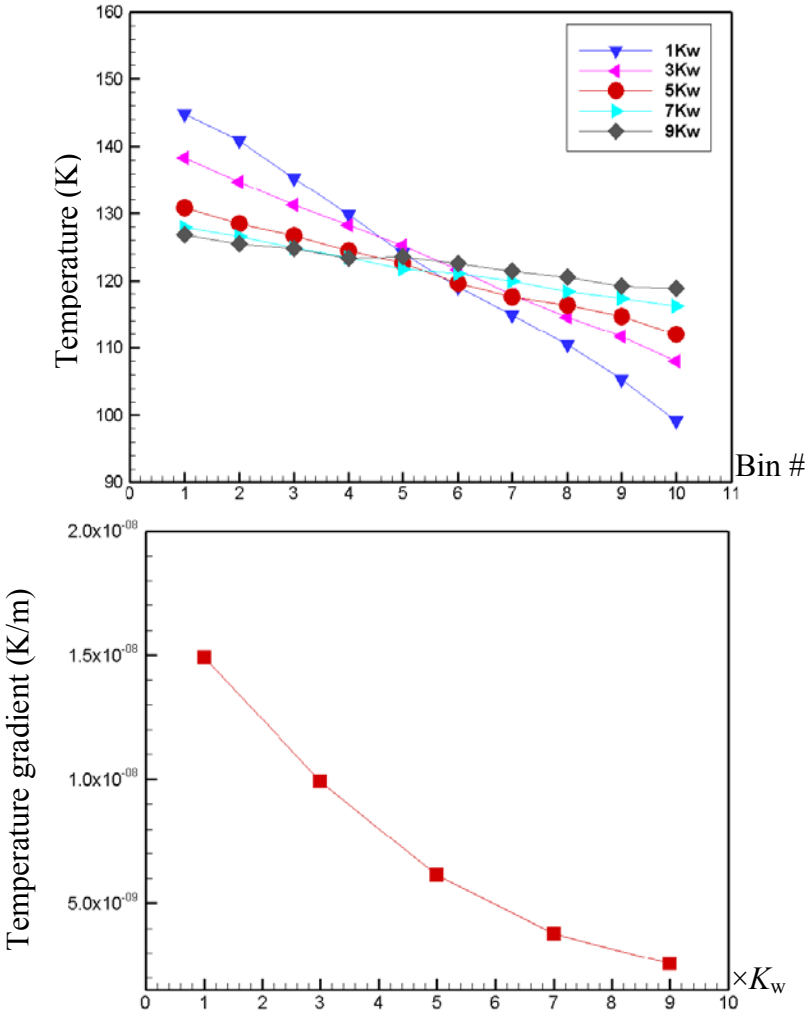

Figure 11. Temperature variation of liquid argon between 90K and 160K walls with various crystal bonding stiffness values ($n \times K_w$, where $K_w = 64\left(4\varepsilon/\sigma^2\right)$) (top). Temperature gradient in the channel decreases with increased crystal bonding stiffness $K = n \times K_w$ (bottom).

Heat flux calculated using equation (9) is shown in Fig. 12 (top), which decreases with increased crystal bonding stiffness. Fig. 12 (bottom) shows the thermal conductivity predicted using Fourier's law, which exhibits constant values, consistent with the values given in Table 1. Temperature profiles, thermal gradients, heat flux, and conductivity are all consistent with the linear constitutive model of Fourier's law. Therefore, the results show that the thermal resistance on the interface solely depends on the interface characteristics, and the thermal conductivity of the liquid is independent of the thermal resistance on the interface. This is an expected result since thermal conductivity is a material property, while the temperature jump and thermal resistance are properties of the interface. Fig. 13 shows temperature jump variation as a function of the crystal bonding stiffness K. High temperature wall (160 K) consistently exhibits higher temperature jumps compared with the wall kept at 90 K. Using thermal gradient and temperature jumps, variation of the Kapitza length as a function of the crystal bonding stiffness is presented in Fig. 14. Thermal resistance and the slip length are slightly larger on the high temperature surface.

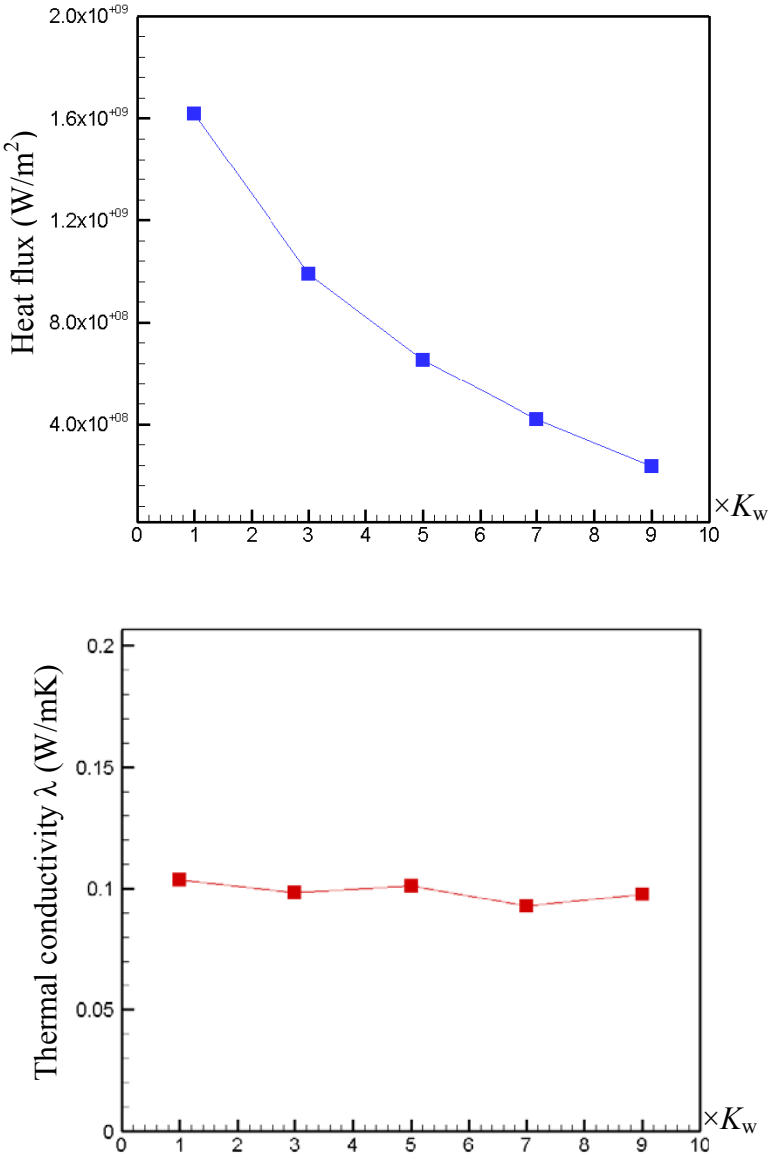

Figure 12. Heat flux and thermal conductivity of liquid argon calculated from Fourier's law. High crystal bonding stiffness K_w decreases the heat flux, while thermal conductivity is maintained a constant.

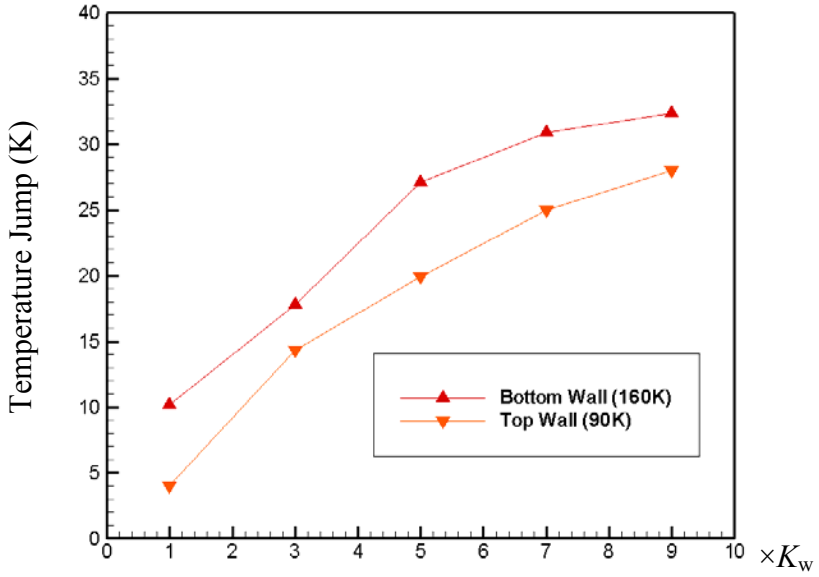

Figure 13. Variation of temperature jump on the interface as a function of the crystal bonding stiffness, obtained for walls kept at 90K and 160K.

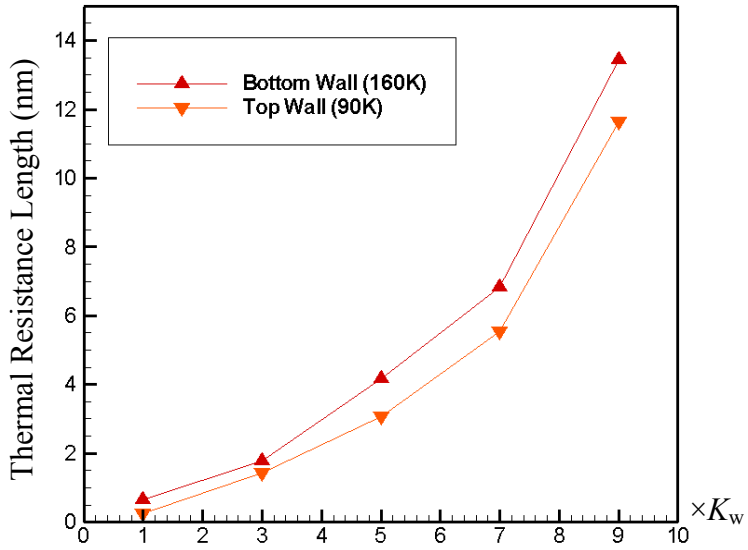

Figure 14. Variation of the thermal resistance length (Kapitza length) as a function of the crystal bonding stiffness, obtained for walls kept at 90K and 160K.

Within the parametric range of the MD simulations, L_K varies from sub-nanometer scales to 13 nm in a channel that is 3.24 nm in height. Slip lengths larger than the channel height are substantial effects that can not be neglected. Overall, increased thermal resistance was observed with increased crystal bonding stiffness *K*, which is related to the thermal oscillation frequency. These results agree with the assumptions in AMM that the dissimilarity of thermal oscillation frequency of material causes thermal resistance on the interface. Stevens *et al.* performed a similar MD study changing the molecular mass to vary the thermal oscillation frequency and compared their results with DMM [35] and they have shown deviations of MD from the DMM predictions. In my results, the thermal resistance length L_K is proportional to $(K_{wall}/K_{liquid})^2$, which scales as $(\omega_{wall}/\omega_{liquid})^4$ when the liquid and solid molecules have equal mass. A simplified analysis of AMM using equation (5) shows that the interface thermal resistance is proportional to $(Z_{wall}/Z_{liquid})^2 \approx (\rho_{wall}\omega_{wall}/\rho_{liquid}\omega_{liquid})^2$, which scales as (K_{wall}/K_{liquid}). Therefore, the MD results explain why AMM under-predicts the interface thermal resistance. As a precautionary statement, note that MD simulations leading to extremely low thermal oscillation frequencies should be avoided to prevent values lower than the melting conditions. In addition, extremely high thermal oscillation frequencies may cause time integration errors, even for small time-steps utilized by the MD method.

Effect of Surface Wettability

Another important microscopic property on the liquid/solid interface is the effect of interaction strength on the interface (i.e. wettability). In MD simulations with a

liquid/solid interface, the effects of interaction strength on the interface and disorder on the lattice crystal's surface are frequently investigated topics. The effect of interaction strength on the interface was studied by changing $\varepsilon_{wf}/\varepsilon$ for the liquid/solid interaction. In order to neglect thermal resistance variations due to crystal bonding stiffness, fixed $K=3K_w$, where the thermal resistance length is about 1.5 ~ 1.8 nm, while ε_{wf} was varied from 0.4ε to 4ε to observe variation of L_K as a function of surface wettability. This modification mainly affects the attractive portion of the molecular potentials. As shown in Fig. 15, strong attractive wall ($\varepsilon_{wf} > 3\varepsilon$) enhances heat transfer on the interface and the thermal resistance length is reduced to almost zero. Moreover, weakened attractive interactions increase the Kapitza length exponentially as shown in Fig. 15 (bottom). Therefore, the Kapitza length varies exponentially with the interaction strength. At fixed K ($K=3K_w$), L_K is approximated $L_K \propto \exp(-1.85\varepsilon_{wf}/\varepsilon_w)$ within the range of $0.4 \le \varepsilon_{wf}/\varepsilon \le 3$, which corresponds to extremely weak and strong interactions, respectively. note that there is a finite limit of interface thermal resistance even if the attractive interaction is reduced to zero. Heat transfer, and hence thermal resistance, should persist under strong repulsive forces that prevent overlap of molecules [31]. Moreover, strong liquid/solid interaction results in layering of fluid molecules which may change thermal conductance [27]. Therefore, the exponential dependence given above should not be utilized at extreme limits.

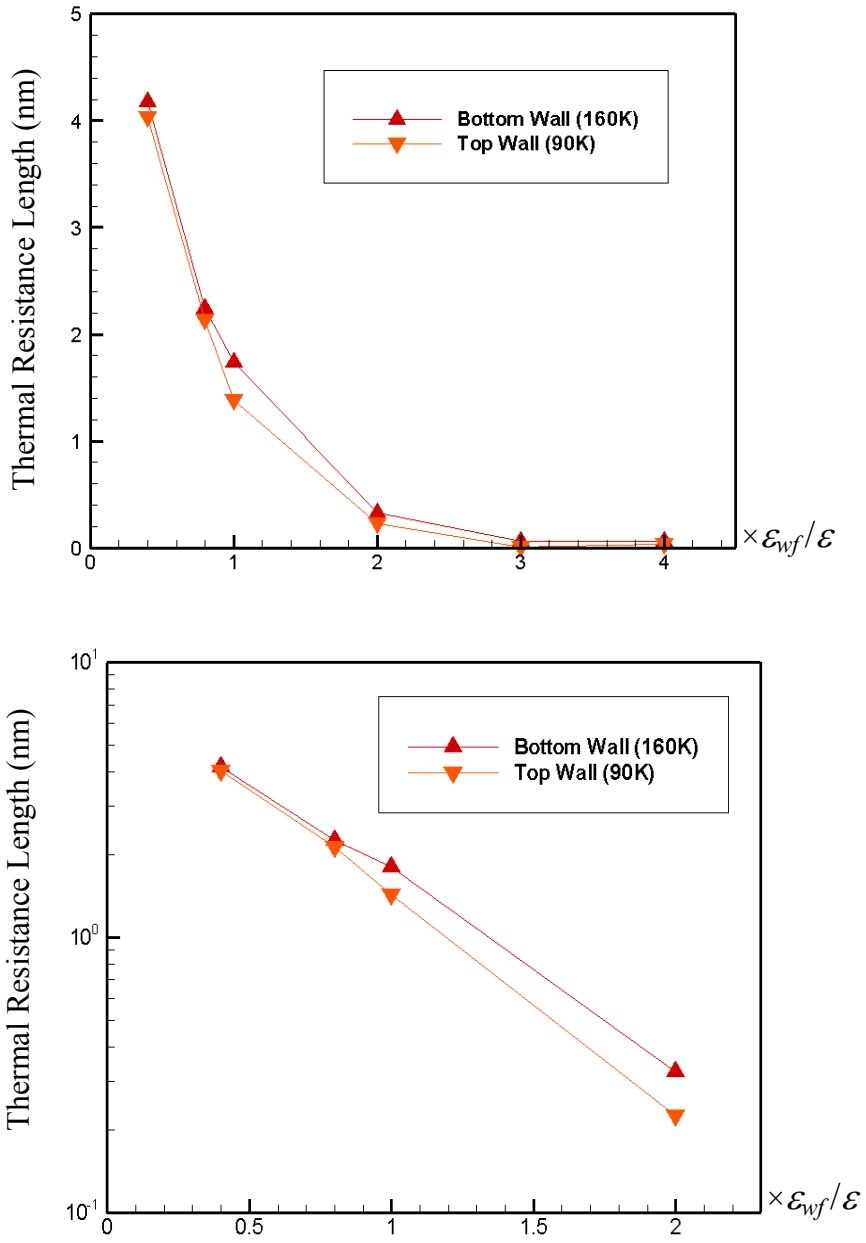

Figure 15. Variation of thermal resistance length as a function of surface wettability ($\varepsilon_{wf}/\varepsilon$) in linear (top) and log (bottom) scales.

Navier Temperature Jump Boundary Condition

In the previous sections, validity of Fourier's law in the nano-channel system was observed. Microscopic properties of interface thermal resistance were analyzed, and have shown that the crystal bonding stiffness and liquid/solid interaction strength have major influences on the interface thermal resistance. In the range of $K_w \le K \le 9K_w$ and $\varepsilon_{wf}/\varepsilon = 1$, $L_K \propto (\omega_{wall}/\omega_{fluid})^4$, while for $0.4 \le \varepsilon_{wf}/\varepsilon \le 3$ and $K=3K_w$, $L_K \propto \exp(-1.85\varepsilon_{wf}/\varepsilon)$. In addition, the Kapitza length is shown to depend on wall temperature (Figs. 13-15). Now hypothesize that the temperature jump $\Delta T_i = f(\frac{\omega_w}{\omega_f}, \frac{\varepsilon_{wf}}{\varepsilon}, T_w, \frac{\partial T}{\partial n})$ should be related to the Kapitza length via equation (4). Since the local thermal gradient is a part of this Navier boundary condition, $L_K = f\left(\frac{\omega_w}{\omega_f}, \frac{\varepsilon_{wf}}{\varepsilon}, T_w\right)$. If locally linear behavior assumed, the Kapitza length is expected to vary as

$$L_K = \alpha(T_w)\left(\frac{\omega_{wall}}{\omega_{fluid}}\right)^4 \exp(-1.85\varepsilon_{wf}/\varepsilon), \tag{13}$$

where $\alpha(T_w)$ is a coefficient with the unit of length scale, and dependent on the wall temperature. Therefore, it is necessary to postulate that within the ranges presented in this work, the Navier temperature jump boundary condition should be given as

$$\Delta T_i = \alpha(T_w)\left(\frac{\omega_{wall}}{\omega_{fluid}}\right)^4 \exp(-1.85\varepsilon_{wf}/\varepsilon)\left.\frac{\partial T}{\partial n}\right|_{liquid}. \tag{14}$$

In order to validate this thermal boundary condition, steady state heat transfer MD simulations were performed at various channel heights (H=3.24nm, 2H, 4H), while keeping L and W unchanged. In simulations, fixed K=3K_w, ε_{wf}=ε, while the top and bottom walls were kept at 160K and 90K, respectively. By keeping the top and bottom walls at a prescribed temperature, $\alpha(T_w)$ was fixed as well. Varying H, the channel height was changed from 3.24 nm to 12.96 nm to obtain different thermal gradients while keeping other variables fixed. Fig. 16 shows that the temperature jump at the interface varies linearly with the temperature gradient, and hence, heat flux. The slope of the figure corresponds to the Kapitza length L_K as described by equation (4). Therefore, interface thermal resistance length L_K is independent of the thermal gradient, while the temperature jump on the interface is linearly proportional to the thermal gradient. Results in Fig 16 validate the analytical form of the boundary condition given in equation (4).

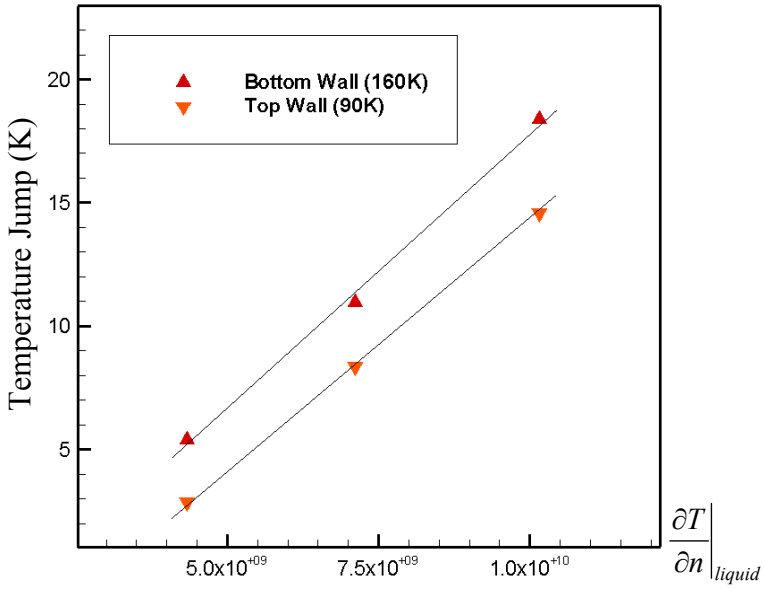

Figure 16. Temperature jump versus the temperature gradient $\frac{\partial T}{\partial n}\Big|_{liquid}$ on the interface. Lines show the least square fit obtained using different channel lengths, with wall temperatures fixed at 90K and 160K.

In order to model $\alpha(T_w)$, the effect of wall temperature on Kapitza length was investigated. For liquid argon, $\alpha(T_w)$ is expected to have linear dependence on the wall temperature, as previously shown in [35]. In order to verify this, $\alpha(T_w)$ was calculated at wall temperatures of 90K, 107.5K, 125K,142.5K and 160K, while keeping the channel height fixed at H=3.24 nm. In Fig. 17 variation of $\alpha(T_w)$ is plotted as a function of the wall temperature (obtained at fixed K=3K_w, ε_{wf}= ε). The results indicate linear variation of α with wall temperature, where a linear fit predicts $\alpha = 0.0038T_w + 0.672$ (fit uses α in nm while T_w in Kelvin). This variation properly explains the higher Kapitza length on

high temperature surfaces in Figs. 13-16. The temperature jump model in equation (14) includes the influence of major microscopic properties of molecular structure and its interaction with fluid molecules. The interface thermal resistance length L_K is proportional to the 4th power of the thermal oscillation frequency ratio, and it is exponentially proportional to the liquid/solid interaction strength. The model also includes macroscopic thermal conditions such as the thermal gradient and wall temperature. This boundary condition can be utilized in continuum formulations, along with the Fourier's law.

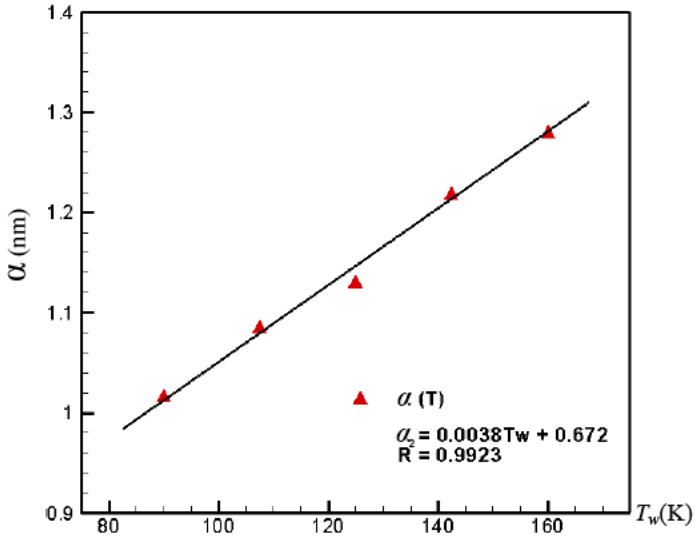

Figure 17. Variation of $\alpha(T_w)$ as a function of the wall temperature. Line shows the least square fit, R^2=1 corresponds to an exact fit.

For further verification, the temperature distribution is obtained based on the analytical solution of the continuum heat conduction equation subjected to equation (14), which results in

$$T(y) = \left(\frac{T_{Low} - T_{High}}{L_{K-High} + L_{K-Low} + H} \right) (y + L_{K-High}) + T_{High}, \quad (15)$$

where $L_{K\text{-}High}$ and $L_{K\text{-}Low}$ correspond to the L_K values on the high and low temperature surfaces, respectively. Temperature distributions from equation (15) have shown excellent agreements with all previous MD results, indicated by dots in the K_w and ε_{ratio} ($\equiv \varepsilon_{wf}/\varepsilon_w$) plane in Fig. 18 (a). Good match was expected, as the model was developed using this particular data. For further verification, MD simulation results were presented with the continuum-based analytical solution for temperature distribution at three more K_w and ε_{ratio} pairs, shown by squares in Fig. 18 (a). The wall temperature was also varied in each case as shown in Fig. 18 (b-d), so that the coupled effects of oscillation frequency, surface wettability and wall temperature on L_K can be verified. Excellent agreements between the MD and analytical solution are demonstrated in Fig. 18 (b-d). Overall, the Navier thermal boundary condition given by equation (14) faithfully predicts the temperature jump on the liquid/solid interface, while the analytical solution given by equation (15) agrees well with the MD predictions.

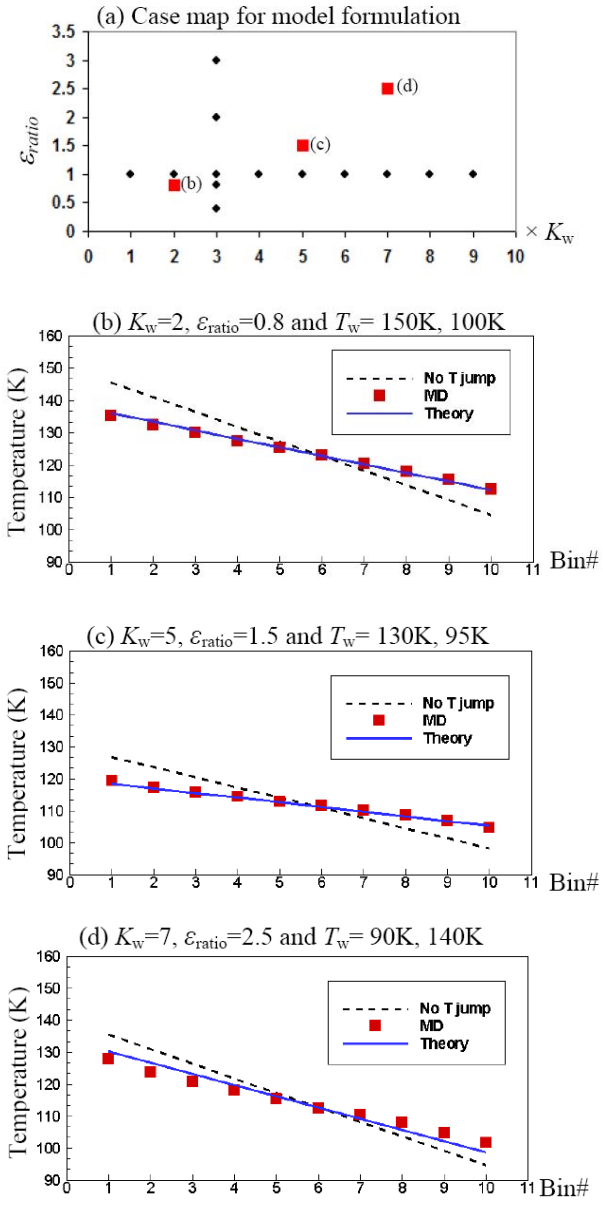

Figure 18. Case-map for verification of the Navier thermal boundary condition for steady state heat transfer problems (dots) along with the three independent verification cases (squares) (a). Results of verification cases (b-d). Theory corresponds to predictions from equation (14).

CHAPTER IV

VISCOUS HEATING IN THE SHEAR FLOW

Over the past decade, significant theoretical and experimental advances are made to describe and measure thermal transport in nano-scale structures, materials and devices [2, 30]. Unless packaged in vacuum, any nano-structure or device will interact with the surrounding fluid. Thus, further advancements in nanotechnology and nano-fluidics as its sub-field require advanced understanding of mass, momentum and energy transport in nano-scale confined fluids. Within the scope of this general problem, momentum transport is studied extensively using the Molecular Dynamics (MD) method [2-5]. Investigations of momentum transport at the liquid-solid interface have shown velocity-slip and -stick conditions depending on the wall-fluid interaction strength, fluid/wall density and shear rate [1, 6, 19, 41].

Surface effects become dominant in nano-scale conduits due to their miniscule dimensions. As a result, nano-scale heat transfer is greatly influenced by the interface thermal resistance (Kapitza resistance) [24]. In addition, thermal equilibrium of the system, macroscopic definition of temperature, and the constitutive laws (i.e., Fourier's law) need to be verified in nano-scale as shown in the previous chapter and references [23, 42, 43]. Given these challenges, it is important to investigate the limitations of the continuum hypothesis in nano-scale heat transfer problems. In the case of flow, driven either by a pressure gradient, boundary motion or body forces, the momentum and heat transport happen simultaneously. Therefore, the coupled molecular modeling of

momentum and heat transport is essential. In addition to the interface thermal resistance effects, work done by the viscous forces heat the fluid, which must be dissipated through the boundary. Current MD models have either physical or computational limitations in coupled momentum and heat transfer simulations. For example, previous MD studies mostly utilized thermostats on the fluid to maintain isothermal conditions. As a result, heat transfer due to viscous heating is completely ignored. Alternatively, direct simulation of thermal transport often requires utilization of large number of wall molecules, connected to external thermal reservoirs to properly dissipate the heat due to viscous heating. In such an approach, the computational load due to the wall molecules remains the same, even though the channel height, and hence, the number of liquid molecules are reduced to model nano-scales.

In this chapter, the coupled momentum and heat transfer is investigated for shear driven nanochannels by utilizing the interactive thermal wall model. The *objectives* for this chapter are to systematically investigate the viscous heating and the resulting temperature profiles as a function of the wall/surface thermal oscillation frequency ratio, surface wettability and the shear rate, and at the same time compare and contrast MD results with the continuum predictions. In order to establish this, it is essential to focus on the local variations of the shear rate, fluid density and viscosity across the nano-channel, which play key roles in continuum modeling of viscous dissipation.

Nanoscale Channel Confined Shear Flow

In order to perform MD simulations of shear driven flow with viscous heating, a total of 578 liquid molecules were simulated in a 3D channel of height (H) 3.24 nm, and

width (W) 2.16 nm and length (L) of 4.32 nm. Fig. 19 shows the schematics and dimensions of the simulation domain that has the interactive thermal walls with perfect FCC crystal (001) surfaces. Periodic boundary conditions are imposed in x and z directions. Temperature and velocity distribution in the fluid is obtained using 10 slab bins (numbered as 1~10) parallel to the walls. The 0^{th} and 11^{th} bins represent the bottom and top walls, respectively. Both wall temperatures are set to 100K as isothermal wall. For the shear driven flow, the characteristic wall velocity (U^*) was set to $U^* = 0.5\sqrt{\varepsilon / m}$.

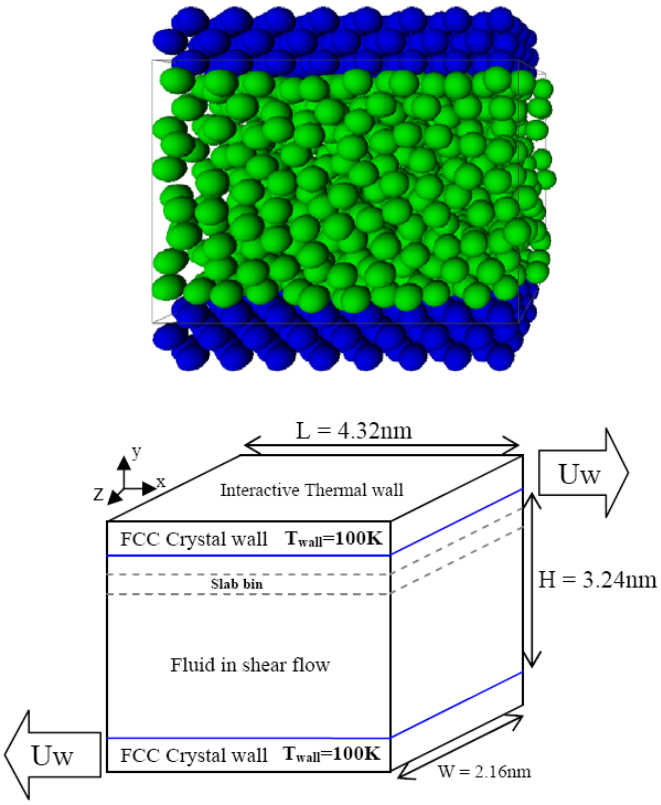

Figure 19. Schematics and dimensions of the simulation domain.

Simulations started from the Maxwell-Boltzmann velocity distribution for both liquid and walls, and ran 2×10^5 time-steps (0.8ns) to reach a steady state, after which another 4×10^5 time steps (1.6ns) were performed for time averaging. Longer time averaging has also been performed to confirm convergence of the velocity profiles and temperature profiles to the steady state. Fig. 20 shows the velocity and temperature profiles from the shear driven flow with wall velocity $U_w = U^*$. For thermal oscillations, intermolecular stiffness for the wall molecules was set as $K=2K_w$ and the surface wettability ($\varepsilon_{wf}/\varepsilon$) was varied from 0.4 to 4. As shown in Fig. 20(a), different surface wettability on the wall/liquid interface results in velocity-slip or -stick on the boundary, which induces different shear-rates in the middle of the fluid even with the same wall velocity configuration. Fig. 20(b) shows the temperature distribution as a result of shear driven flow. Weak and normal wetting wall cases result in almost parabolic temperature distribution, which would be expected from shear driven flow of a Newtonian fluid. Moreover, temperature jump as a result of the Kapitza resistance is also visible with the exception of the strong wetting surface case.

The surface wettability (wall/fluid interaction strength) varies the shear rate due to the velocity-slip and -stick phenomena, as shown in Fig. 20(a); and such differences in the shear rate cause different temperature profiles even for the same wall velocity conditions. In addition, for the strong wetting case, both the temperature profile and velocity profile shows non-linear distribution near the boundary, but the weak wetting case shows almost linear velocity profile and smooth parabolic temperature profile with temperature jump on the boundary. Therefore, proper boundary conditions for the

temperature jump on the interface with the continuum energy equation may enable the prediction for the temperature profile in nano channels for certain cases.

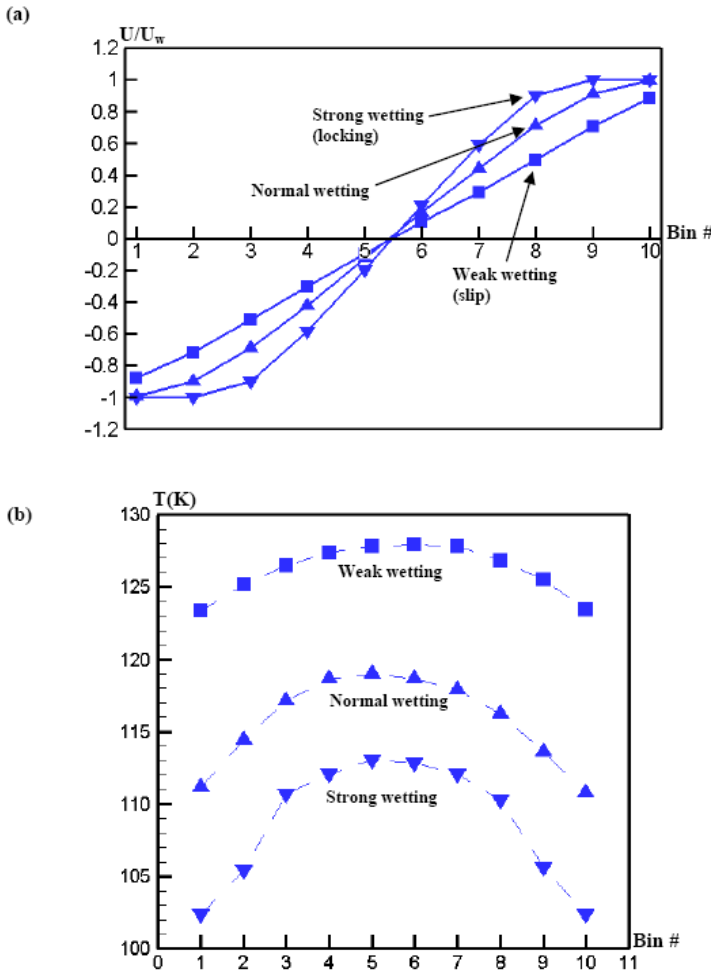

Figure 20. Velocity (a) and temperature profiles (b) with strong ($\varepsilon_{wf}/\varepsilon = 4$), normal ($\varepsilon_{wf}/\varepsilon = 1$), and weak ($\varepsilon_{wf}/\varepsilon = 0.4$) surface wettability and $K=2K_w$.

Shear Rate, Density and Viscosity Distribution

Before applying the continuum approach to the nanoscale channel flow with weak wetting walls ($\varepsilon_{wf}/\varepsilon$ =0.4), it is essential to investigate the distribution of local density (ρ), local dynamic viscosity (μ) and local shear rate ($\dot{\gamma}$) predicted as a result of MD simulations. For the viscosity measurement, there are two common methods. One utilizes a body force applied to all fluid molecules, which generates a Poiseuille flow profile. Measurement of the maximum velocity for a no-slip simulation enables calculation of the viscosity using the continuum solution, as described in References [18, 21]. Another method is to utilize the stress tensor (σ_{xy}) including the molecular level descriptions. The dynamic viscosity of liquid in molecular system is defined as the ratio of the shear component of the stress tensor (σ_{xy}) and the applied shear rate in fluid mechanics,[44]

$$\mu = -\frac{\langle \sigma_{xy} \rangle}{\dot{\gamma}}, \tag{16}$$

where

$$\sigma_{xy} = \frac{1}{\Omega}\left(\sum_{i=1}^{N} \frac{P_{xi} P_{yi}}{m_i} + W_{xy} \right), \tag{17}$$

where $P_{ni} = v_n m_i$, v is the velocity of i^{th} molecule, N is the number of molecules, Ω is the volume of bin, W_{xy} is the virile of the material defined as $W_{xy} = \frac{1}{2}\sum_{i,j}^{N} r_{xij} F_{yij}$. The developed MD code successfully calculated the viscosity of liquid argon utilizing both methods as shown in Table 2, which includes comparisons with published values in the

literature.[11] The error ranges shown for the Poiseuille flow case is due to the ambiguity in the definition of the boundary line that results in no-slip on the boundaries.[45]

Table 2. Dynamic viscosity (μ) of liquid argon around 100K and ρ^*= 0.8. (1 cP = 1 Pa·s×10^{-3}).

Viscosity from MD, Poiseuille flow normal wetting ($\varepsilon_{wf}=\varepsilon$)	Viscosity from MD, shear flow normal wetting ($\varepsilon_{wf}=\varepsilon$)	Viscosity from MD, Koplick *et al.* [11, 45]	Viscosity from Experiments in [11]
0.185 ± 0.008 cP	0.194 cP	0.18 ± 0.027 cP	0.2 cP

In order to apply the continuum analysis to solve for the temperature distribution, the energy equation for 1-D shear driven Newtonian fluid flow is used

$$\frac{d^2T}{dy^2} = -\frac{\mu}{\lambda}\left(\frac{du}{dy}\right)^2, \tag{18}$$

where each of the terms on the RHS, such as the density ρ, dynamic viscosity μ, and the shear rate ($\frac{du}{dy} = \dot{\gamma}$) are constants. Alternatively, the dissipation rate given by the RHS of equation (18) should be approximately a constant. The thermal conductivity (λ) was already investigated and shown to be a constant along the channel in a previous chapter. In the following, the investigation for the local behavior of ρ, μ and $\dot{\gamma}$ will be presented.

In order to investigate the density distribution in the channel, it is very important to elucidate the ambiguous definition of wall boundary. For convenience, the boundary line is defined at the center of aligned wall molecules at the 1st layer adjacent to the fluid molecules, and kept this definition for the whole analysis. In this definition of the wall

boundary, some of the 1st bin volume is occupied by the wall molecules. Moreover, the maximum penetration depth of the fluid molecules due to the wall force field is unknown, making it difficult to determine the effective bin volume. Ambiguity in the actual bin volume near the boundary induces errors in definition of fluid properties such as density or the dynamic viscosity predicted using equation (16). As shown in Fig. 21, a more detailed molecular distribution can be obtained along the channel if the bins are about 10 times smaller than the molecular diameter.

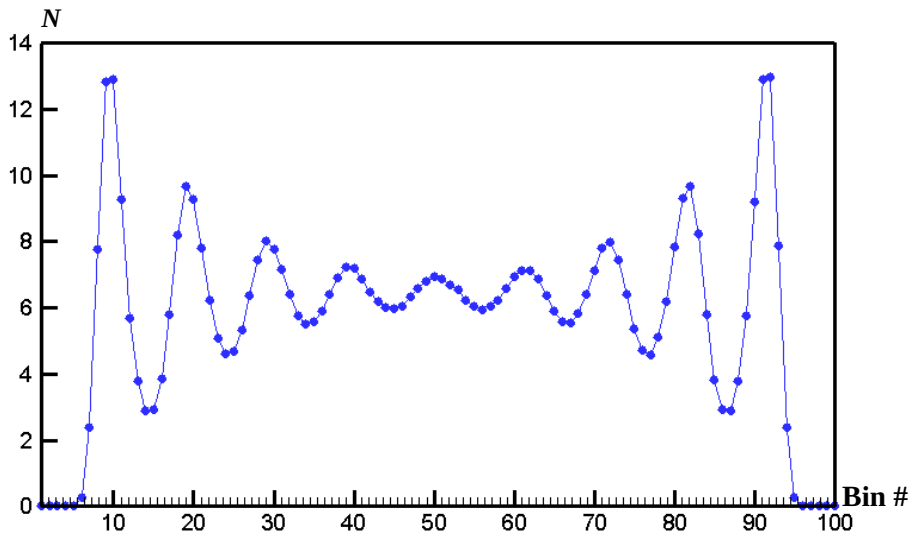

Figure 21. Number of molecule (N) distribution in 3.4 nm channel with weak ($\varepsilon_{wf}/\varepsilon$ = 0.4) surface wettability and K=2K_w, using 100 bins across the channel.

Under such conditions, the first four bins are occupied by wall molecules (Fig. 22 a), and hence, the number density of liquid molecules is zero in these finer bins (Fig. 22 b). The

void fine-bins indicate that the liquid molecules can only occupy (approximately) 60% of the first bin. For this fact, density distribution in the nano-channel can be corrected in the first bin neighboring the walls.

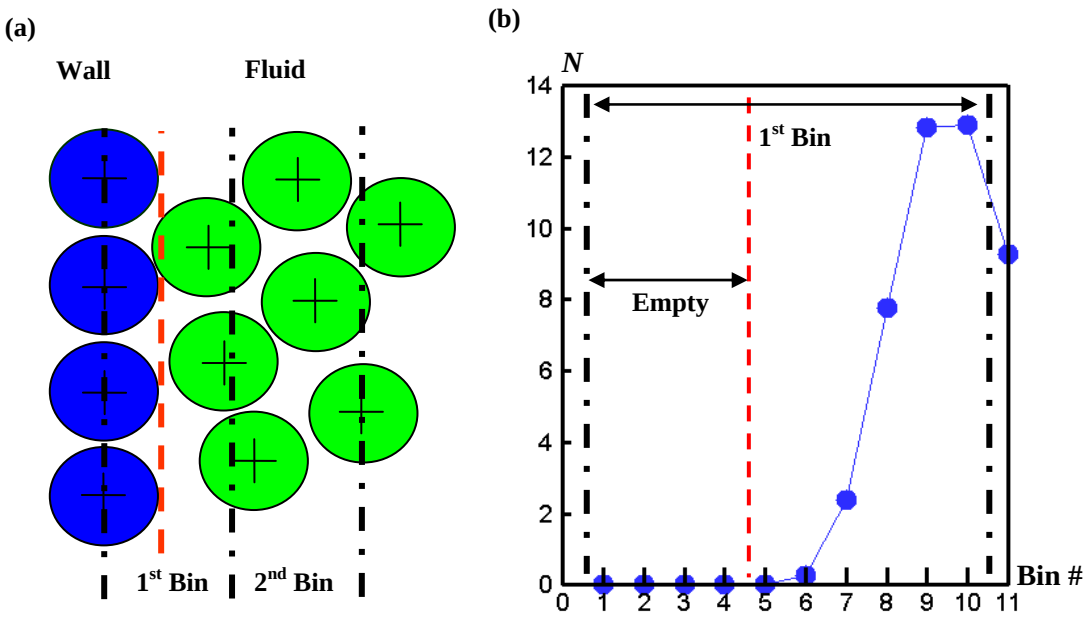

Figure 22. (a) Schematics of the molecules within the first two bins near the wall. (b) Molecular distribution within 1st bin. Empty sub-bins near the wall are noteworthy.

The result of this correction is shown in Fig 23, where spatial variations in density are reduced significantly. In defense of this approach it is necessary to indicate two important points. First, density as mass per unit volume is a continuum concept, which is destined to break-down in scales (bin sizes) smaller than a molecular diameter (σ). Due to the finite size of the molecules one would register density fluctuations, regardless of

the time used for averaging the results. This is indeed shown in Fig. 21. Such layering effects are important to investigate the radial distribution function and the structure of molecular distributions. However, these should not be used to describe "density" in the continuum sense. Second, the molecular diameter (σ) is the intrinsic length scale in MD simulations, and therefore, seeking "continuum" definitions for scales smaller than σ is an inconsistency.

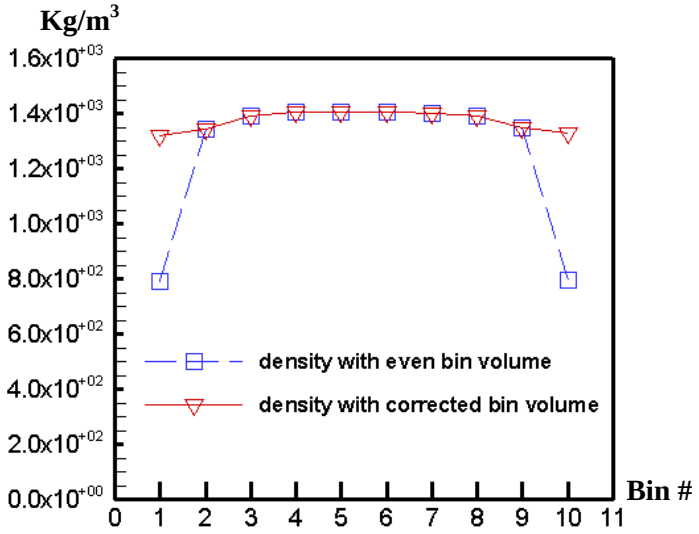

Figure 23. Density (ρ) distribution in the channel with and without the corrected volume of the 1st bin.

In order to investigate the viscosity distribution, the kinematic viscosity (v) is utilized rather than the dynamic viscosity (μ). This is because the kinematic viscosity can be calculated based on the average number of molecules of the bin, instead of the bin volume used in the definition of μ as shown in equations (16) and (17). Since the

kinematic viscosity is $\nu = \frac{\mu}{\rho}$, and the density is $\rho = \frac{Nm_a}{\Omega}$, the kinematic viscosity becomes

$$\nu = -\frac{\left\langle \sum_{i=1}^{N} \frac{P_{xi} P_{yi}}{m_i} + \frac{1}{2} \sum_{i,j}^{N} r_{xij} F_{yij} \right\rangle}{\dot{\gamma}} \frac{1}{Nm}. \tag{19}$$

In this equation, the volume (Ω) used in equation (17) cancels with volume in the definition of the density, making the kinematic viscosity definition independent of the bin volume. This directly avoids the problem in the definition of density due to the 40% void volume of the first bins neighboring the walls. Using the definition in equation (19), the precise number of molecules (*N*) can be obtained through time averaging. Therefore, it is possible to compute the kinematic viscosity distribution precisely including the bins on the boundary.

Fig. 24 shows the local shear rate and local kinematic viscosity distributions in the channel. The local shear rate was obtained using 1st order finite difference approximation between the bin velocities. As shown in Fig. 24(a) the local shear rate in the weak wetting wall cases decreases near the boundary, even though the velocity profile is (almost) linear (see Fig. 20 a). Moreover, the kinematic viscosity increases near the boundaries as shown in Fig. 24 b. This is expected even for weaker wall attractions, since the attractive forces from the well defined FCC structure walls still affect the nearby fluid molecules.

Variation of the shear rate and kinematic viscosity as a function of the surface wettability are shown in Fig. 25. The results consistently show that the discrepancies

between the near wall and channel center values of the shear rate and kinematic viscosity increases with increased surface wettability. Variations in the kinematic viscosity are noteworthy. For the $\varepsilon_{wf}/\varepsilon = 0.6$ case, kinematic viscosity near the moving surfaces are almost twice the values observed in the channel center, while the shear rate at the channel center increases 1.67 folds, when compared to the value near the boundaries. This is a direct result of more liquid molecules being dragged by the moving walls due to the increased surface wettability.

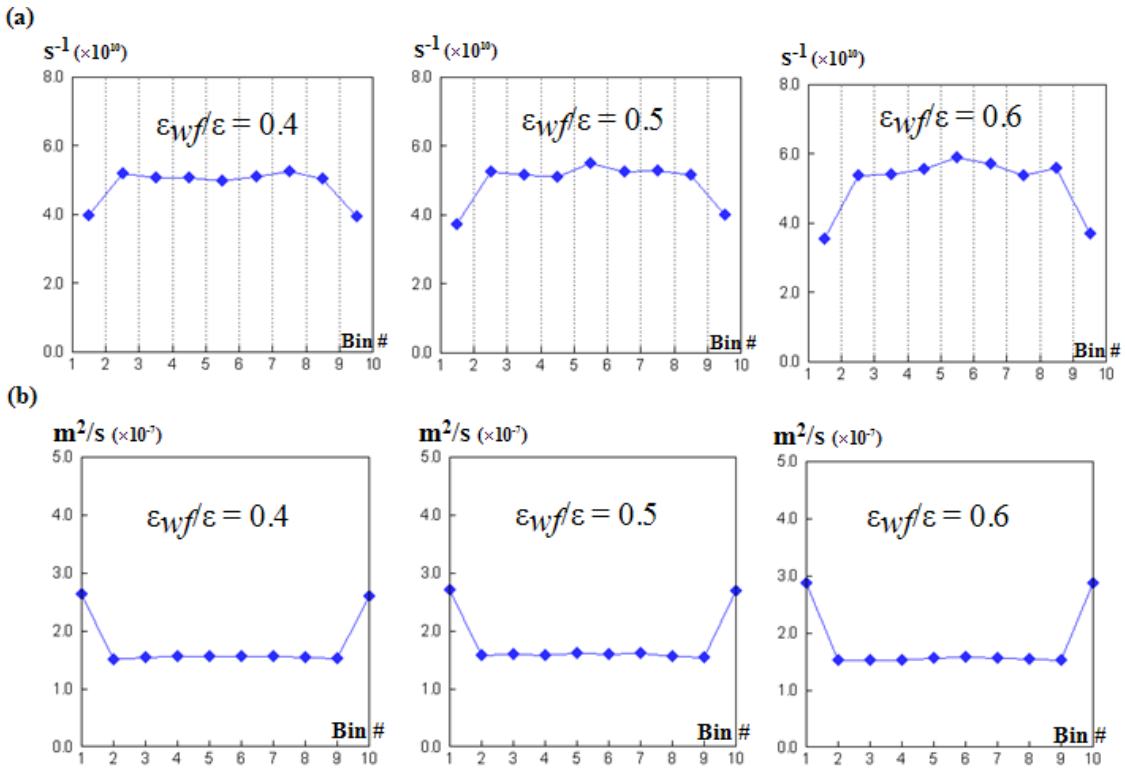

Figure 24. Distribution of the shear rate ($\dot{\gamma} = \frac{\partial u}{\partial y}$) (a), and kinematic viscosity (b) in the nano-channels as a function of the surface wettability.

Results in Fig. 24 have shown almost constant kinematic viscosity across the channel with the exception of the bins closest to the walls, while a similar behavior is valid for the shear rates. On the other hand, Fig. 25 has shown that the differences between the wall and channel center values of the shear rate and kinematic viscosity increase with $\varepsilon_{wf}/\varepsilon$.

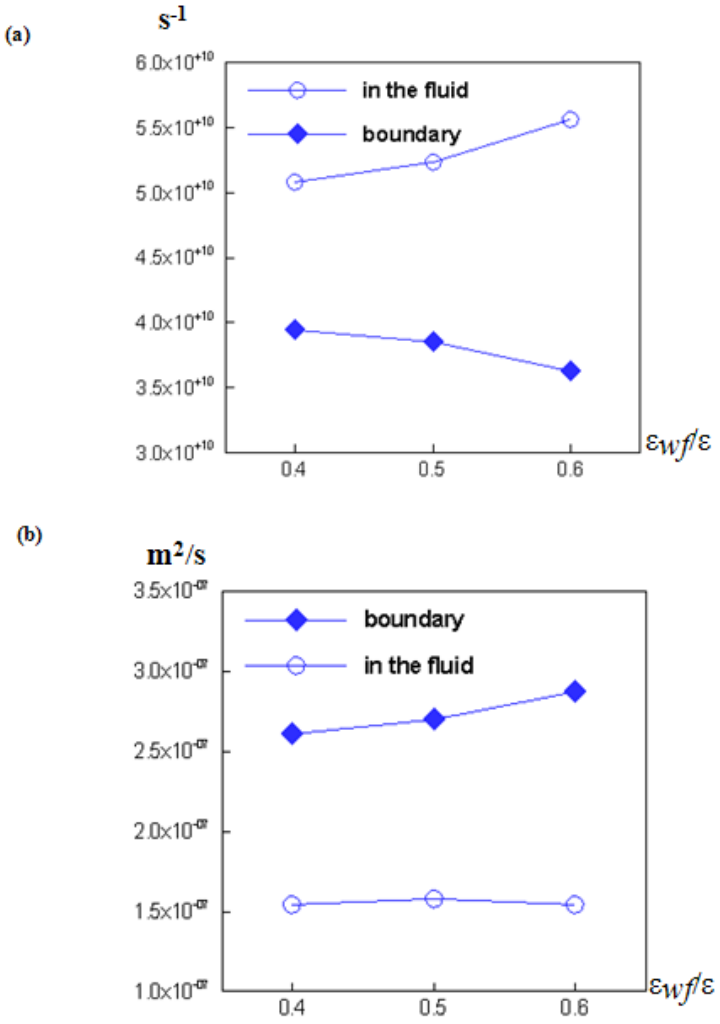

Figure 25. Shear rate ($\dot{\gamma} = \frac{\partial u}{\partial y}$) (a), and kinematic viscosity (b) at the boundary and middle of the channel as a function of the surface wettability.

These are definite deviations from the behavior of classical Newtonian fluid in a liner shear driven (Couette flow). Given these discrepancies, it is necessary to investigate spatial variations in the dissipation rate, given by the right hand side of equation (18). In order not to include the local density variations, the Fig. 26 shows the spatial variation of $\nu\dot{\gamma}^2$ normalized by its channel average value $\left[\nu\dot{\gamma}^2\right]_{avg}$ where $\dot{\gamma} = \partial u/\partial y$.

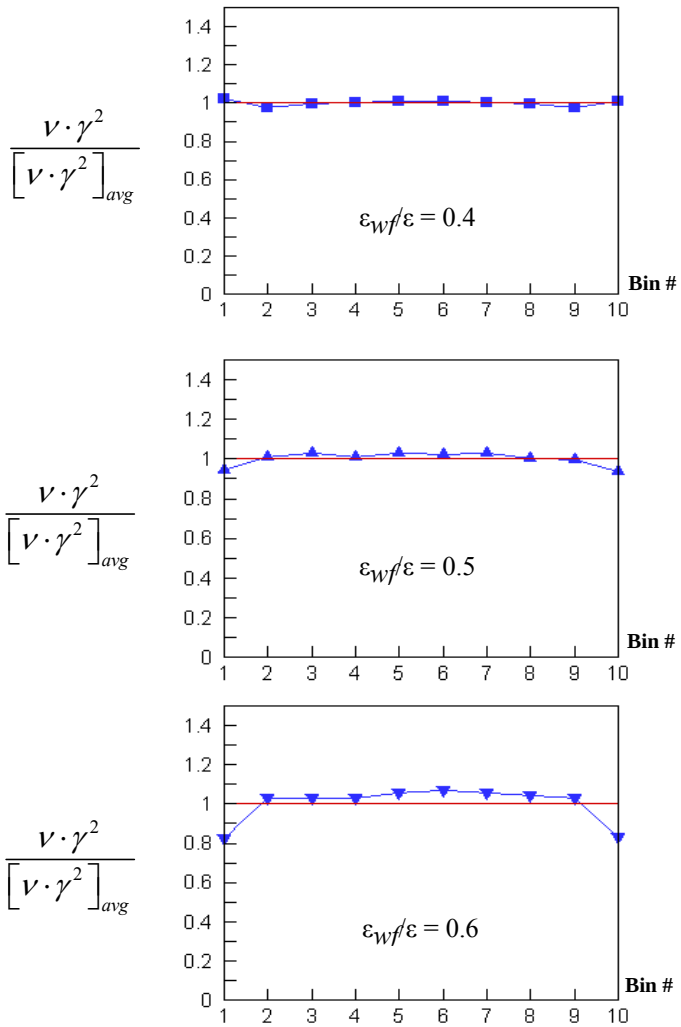

Figure 26. Variation of the normalized $\nu\cdot\dot{\gamma}^2$ value across the nano-channels for different surface wettability values.

Surprisingly, $\nu\dot{\gamma}^2$ is almost a constant along the channel with less than 10% variations for the weak interaction cases ($\varepsilon_{wf}/\varepsilon \leq 0.5$). However, 20% variation is observed near the walls for $\varepsilon_{wf}/\varepsilon = 0.6$. For the quantification purposes, Fig. 27 presents $\left[\nu\dot{\gamma}^2\right]_{avg}$ as a function of the surface wettability, where a linear increase in $\left[\nu\dot{\gamma}^2\right]_{avg}$ is observed with increased $\varepsilon_{wf}/\varepsilon$. More specifically 15% increase in $\left[\nu\dot{\gamma}^2\right]_{avg}$ is observed by increasing the surface wettability from 0.4 to 0.6, which is a substantial effect for such small variations in the $\varepsilon_{wf}/\varepsilon$ values. Therefore, more viscous heating is expected in higher surface wettability channels, even though the nano-channel surfaces are sheared with a constant velocity.

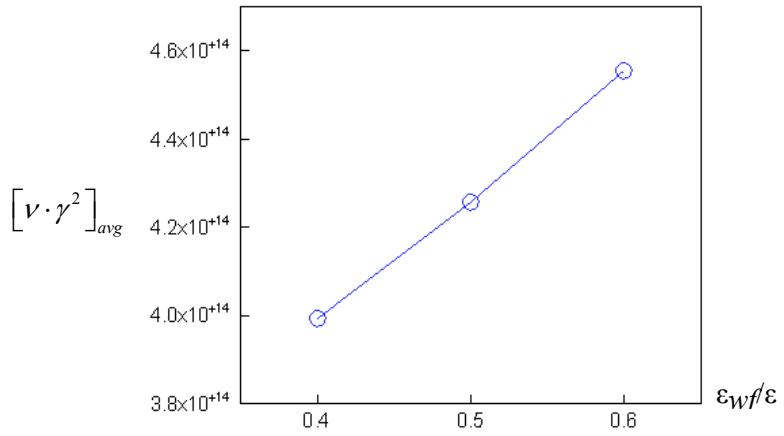

Figure 27. Variation of the average $\nu \cdot \dot{\gamma}^2$ value as a function of the surface wettability.

Using Figs. 24 to 26, unique deviations from the Newtonian fluids behavior is observed at the kinematic viscosity and shear rate in nano-channels. If one can

systematically formulate these variations, it could be ultimately possible to describe the momentum transport in nano-channels in the form of a continuum formulation based on proper constitutive laws and boundary conditions. In addition, it may be possible to couple this with a proper thermal transport model.

Theoretical Prediction of Temperature Profile

In the rest of this chapter, the coupling between the momentum and heat transport will be show by investigating the temperature profile in the nano-channel as a result of the viscous heating effects. For this purpose, $\left[\nu\dot{\gamma}^2\right]_{avg}$ will be utilized for each $\varepsilon_{\omega f}/\varepsilon$ case, which shows less than 10% spatial variations for $\varepsilon_{\omega f}/\varepsilon$= 0.4 and 0.5 cases, and 20% variation for the $\varepsilon_{\omega f}/\varepsilon$ = 0.6 case. Encouraged by these relatively small spatial variations, equation (18) can be rewritten as

$$\frac{d^2T}{dy^2} = -\frac{\rho}{\lambda}\left[\nu\left(\frac{du}{dy}\right)^2\right]_{avg} = -\frac{\rho}{\lambda}\left[\nu\dot{\gamma}^2\right]_{avg}, \tag{20}$$

where $\left[\nu\dot{\gamma}^2\right]_{avg}$ is a constant. This equation is subjected to the temperature jump and symmetry boundary conditions on the channel walls and the channel center, respectively. The rate of work done by the shear stresses induces viscous heating on the fluid, while the system reaches to a steady state by dissipation of heat through the channel walls. The result is a parabolic temperature distribution with a jump due to the interface thermal resistance, given as

$$T(y) = -\frac{A}{2}y^2 + \frac{AH}{2}y + T_W + L_K\frac{AH}{2}, \tag{21}$$

where $A=(\rho/\lambda)\left[\nu\dot{\gamma}^2\right]_{avg}$ and L_K is the Kapitza length given by equation (13). In Fig. 28, the temperature distributions in nano-channels obtained by the continuum-based analytical solutions and MD simulations are presented. The verification cases are chosen by varying $2K_w \le K \le 3K_w$, and by moving the top and bottom walls of the channel with velocities of $U^* \le U_w \le 0.5\ U^*$ in opposite directions. Hence, this figure shows temperature profiles obtained by varying the shear rate, surface wettability ratio and the stiffness of the wall molecules.

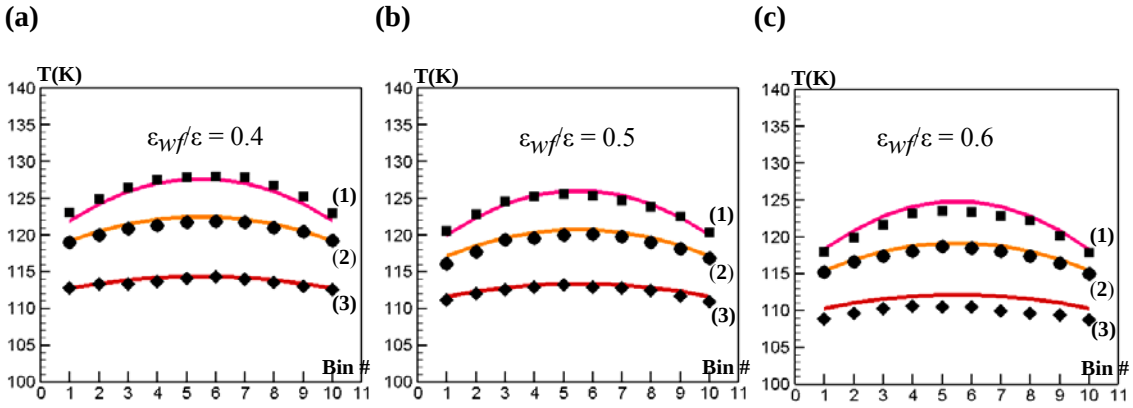

Figure 28. Temperature profiles in shear driven flow calculated by MD (symbols) and predicted by the theory (lines) obtained for various $\varepsilon_{wf}/\varepsilon$ values, shear rates and K values. (1) $K=2K_w$, $U_w=U^*$,(2) $K=2.5K_w$, $U_w=0.75U^*$ and (3) $K=3K_w$, $U_w=0.5U^*$ where $U^*=0.5\sqrt{\varepsilon/m}$.

Excellent agreements between the MD and analytical solutions are demonstrated in Figs. 28 (a) and (b). The temperature jumps are reduced by increasing K values, as expected from equation (14). Temperature profiles for the $\varepsilon_{wf}/\varepsilon = 0.6$ case, in Fig. 28 (c), shows differences from the continuum predictions due to the larger spatial variations in $\nu(\partial u/\partial y)^2$. However, the agreement between the MD and continuum predictions can still be acceptable. Overall, the Navier-type thermal boundary condition given by equation (14) faithfully predicts the temperature jump on the liquid/solid interface, while the analytical solution given by equation (21) shows excellent agreements with the MD simulations.

CHAPTER V

CONCLUSIONS

In this study, a molecular dynamics algorithm based on the 6-12 Lennard Jones potential interactions are developed along with a new interactive thermal wall model, which allows coupled momentum and energy transport simulations in nano-scale channels. Unlike the model used in previous studies, which often concentrated on the velocity slip as a function of the interaction potential, shear rate and the density of wall molecules, the new interactive thermal wall model can impose isothermal boundary conditions on the channels walls by applying a thermostat on each wall layer. The new model does not affect the momentum transport, and hence, it allows coupled momentum and energy transport simulations in nano-channels.

Using MD simulations employing the new interactive thermal wall model, systematic studies of heat conduction in nano-channels were performed. The current study was limited to liquid argon at fixed density, which was modeled using the 12-6 Lennard-Jones interaction potential. Channel walls were modeled as perfect FCC crystal (001) surfaces with no electrical charges or any other long-distance force fields. Within this simplified system, Fourier's law of heat conduction was validated, which resulted in linear temperature distribution with constant thermal conductivity, as verified by the Green-Kubo method. Validity of continuum hypothesis and linear constitutive law in nano-channels as small as 3.24 nm, which resulted in extremely large heat flux, are indeed surprising. Such behavior can be due to the utilization of the 12-6 Lennard-Jones

interaction potential. More complex molecules, requiring other interaction potentials or inclusion of long-range forces or polarity may induce deviations from current results.

In heat transfer studies, temperature profiles consistently exhibited jumps at the liquid/solid interface, which corresponded to Kapitza resistance. Based on this observation, systematic studies of Kapitza length were performed as a function of the surface wettability ($\varepsilon_{wf}/\varepsilon$) and thermal oscillation frequency (K_w). Simulations were performed within the range of $K_w \le K \le 9K_w$ and $0.4 \le \varepsilon_{wf}/\varepsilon \le 3$, and it was consistently observed that the Kapitza length increases with the increased thermal oscillation frequency and decreased surface wettability. These results are qualitatively similar to the predictions of AMM and MD. However, quantitative differences exist. For example, AMM predicts thermal resistance proportional to (K_{wall}/K_{liquid}), while MD predicts scaling with $(K_{wall}/K_{liquid})^2$, which may be useful in explaining deviations of AMM results from experiments at high temperatures. Similar deviations between DMM and MD were also reported [35]. Verification of MD predictions at high temperatures is out of scope of the current work. Our MD simulations have shown exponential variation of L_K with $\varepsilon_f/\varepsilon_w$, similar to the other MD results in [31], where exponential variation of Kapitza resistance as a function of surface wettability was shown for $\varepsilon_{wf}/\varepsilon \le 1$. It must be reemphasized that exponential variation of L_K with $\varepsilon_{wf}/\varepsilon$ can not be sustained for $\varepsilon_{wf}/\varepsilon$ <0.4, since there will be thermal resistance even when the attractive portion of liquid/wall interaction forces is reduced to zero.

Using MD results within the range of $K_w \leq K \leq 9K_w$ and $0.4 \leq \varepsilon_{wf}/\varepsilon \leq 3$, and by varying the channel dimensions and wall temperatures, an empirical model was developed for L_K as a function of surface wettability, thermal oscillation frequency and surface temperature. This model is combined with a thermal boundary condition, which enabled us to predict the temperature distribution in nano-channels using continuum based models. The resulting temperature jumps are shown to agree with MD predictions at arbitrarily chosen K, $\varepsilon_f/\varepsilon_w$ and T_w values. The boundary condition includes not only the macroscopic thermal conditions of the system, but also the influences of the molecular structure and its interactions. Such boundary conditions can be further developed to understand the complex interface thermal resistance phenomena. Investigation of the effects of other microscopic properties related to the molecular structure such as the liquid/solid density, direction of the lattice crystal, crystallographic defects, layering of liquid molecules on the solid surface, electrical charges, complex and/or polar fluids will be the topic of future research.

Detailed MD simulations of heat and momentum transfer in shear driven nano-scale flows were performed, where heat transfer is due to the work done by viscous stresses. Based on these simulations, the following were observed:

1. In the definition of density one must consider bin sizes that are comparable to, or larger than the molecular diameter σ.

2. Density in the bins immediately neighboring the walls should be corrected for the volume occupied by the wall molecules, which substainally reduces the spatial variations in density.
3. Both the shear rate and kinematic viscosity show spatial variations across the nano-channel. Kinematic viscosity near the walls is increased and the shear rate is decreased due to the influence from the wall, compared to their values observed in the channel center. These are deviations from the Newtonian fluid.
4. For surface wettabilities smaller than 0.6, spatial variations in the viscous dissipation are lower than 10%. This allows integration of the heat equation with an approximately constant source term, resulting in parabolic temperature profiles with temperature jumps at the solid/liquid interface.
5. The temperature profiles predicted by the continuum model subjected to our phenomenological temperature jump model agree with the MD simulation results.

Further understanding of the coupling between the momentum and energy transport for $\varepsilon_{\omega f}/\varepsilon > 0.6$ requires detailed studies of the shear rate, density and kinematic viscosity variations in nano-channels along with the characterization of the velocity-slip and -stick effects on the surface. Our Kapitza length model is a function of the surface wettability ($\varepsilon_{\omega f}/\varepsilon$), wall crystal stiffness (K), and wall temperature. Among these variables only the surface wettability plays an important role in the momentum transport. Therefore, our thermal model could be easily incorporated for nano-scale flow cases, once a continuum-based model is developed for the momentum transport.

Overall, deviations from the continuum behavior for simple fluids are mainly due to the effect of the force field and the molecular structure of the walls, which affect length-scales on the order of a few molecular diameters. These effects could be incorporated to the velocity slip/stick boundary conditions with some corrections of fluid density near the surfaces. Away from the walls, rest of the liquid experiences the continuum behavior for simple Lennard-Jones fluids.

REFERENCES

[1] N. V. Priezjev, A. A. Darhuber, and S. M. Troian, "Slip behavior in liquid films on surfaces of patterned wettability: Comparison between continuum and molecular dynamics simulations," *Physical Review E,* vol. 71, p. 041608, Apr 2005.

[2] G. Karniadakis, A. Beskok, N. Aluru, S. S. Antman, J. E. Marsden, and L. Sirovich, "Microflows and Nanoflows Fundamentals and Simulation," in *Interdisciplinary Applied Mathematics, 29* New York, NY: Springer, 2005.

[3] M. Cieplak, J. Koplik, and J. R. Banavar, "Applications of statistical mechanics in subcontinuum fluid dynamics," *Physica a-Statistical Mechanics and Its Applications,* vol. 274, pp. 281-293, Dec 1 1999.

[4] J. Koplik and J. R. Banavar, "Continuum Deductions from Molecular Hydrodynamics," *Annual Review of Fluid Mechanics,* vol. 27, pp. 257-292, 1995.

[5] D. J. Evans and W. G. Hoover, "Flows Far from Equilibrium Via Molecular-Dynamics," *Annual Review of Fluid Mechanics,* vol. 18, pp. 243-264, 1986.

[6] P. A. Thompson and S. M. Troian, "A general boundary condition for liquid flow at solid surfaces," *Nature,* vol. 389, pp. 360-362, Sep 25 1997.

[7] M. Cieplak, J. Koplik, and J. R. Bavanar, "Molecular dynamics of flows in the Knudsen regime," *Physica a-Statistical Mechanics and Its Applications,* vol. 287, pp. 153-160, Nov 15 2000.

[8] J. C. Maxwell, "On stress in rarefied gases arising from inequalities of temperature " *Philos. Trans. R. Soc. Lon,* vol. 170, pp. 231-256, 1879.

[9] G. A. Bird, *Molecular gas dynamics and the direct simulation of gas flows*. Oxford: Clarendon Press 1994.

[10] P. A. Thompson and M. O. Robbins, "Shear-Flow near Solids - Epitaxial Order and Flow Boundary-Conditions," *Physical Review A,* vol. 41, pp. 6830-6837, Jun 15 1990.

[11] J. Koplik, J. R. Banavar, and J. F. Willemsen, "Molecular-Dynamics of Fluid-Flow at Solid-Surfaces," *Physics of Fluids a-Fluid Dynamics,* vol. 1, pp. 781-794, May 1989.

[12] H. C. Andersen, "Molecular-Dynamics Simulations at Constant Pressure and-or Temperature," *Journal of Chemical Physics,* vol. 72, pp. 2384-2393, 1980.

[13] H. J. C. Berendsen, J. P. M. Postma, W. F. Vangunsteren, A. Dinola, and J. R. Haak, "Molecular-Dynamics with Coupling to an External Bath," *Journal of Chemical Physics,* vol. 81, pp. 3684-3690, 1984.

[14] S. Nose, "A molecular dynamics method for simulations in the canonical ensemble (Reprinted from Molecular Physics, vol 52, pg 255, 1984)," *Molecular Physics,* vol. 100, pp. 191-198, Jan 2002.

[15] S. Nose, "A Unified Formulation of the Constant Temperature Molecular-Dynamics Methods," *Journal of Chemical Physics,* vol. 81, pp. 511-519, 1984.

[16] W. G. Hoover, "Canonical Dynamics - Equilibrium Phase-Space Distributions," *Physical Review A,* vol. 31, pp. 1695-1697, 1985.

[17] M. Sun and C. Ebner, "Molecular-Dynamics Simulation of Compressible Fluid-Flow in 2-Dimensional Channels," *Physical Review A,* vol. 46, pp. 4813-4818, Oct 15 1992.

[18] M. Sun and C. Ebner, "Molecular-Dynamics Study of Flow at a Fluid-Wall Interface," *Physical Review Letters,* vol. 69, pp. 3491-3494, Dec 14 1992.

[19] M. Cieplak, J. Koplik, and J. R. Banavar, "Boundary conditions at a fluid-solid interface," *Physical Review Letters,* vol. 86, pp. 803-806, Jan 29 2001.

[20] J. Koplik and J. R. Banavar, "Slip, immiscibility, and boundary conditions at the liquid-liquid interface," *Physical Review Letters,* vol. 96, p. 044505, Feb 3 2006.

[21] M. P. Allen and D. J. Tildesley, *Computer simulation of liquids*. New York: Oxford University Press, 1989.

[22] D. J. Evans and B. L. Holian, "The Nose-Hoover Thermostat," *Journal of Chemical Physics,* vol. 83, pp. 4069-4074, 1985.

[23] A. Tenenbaum, "Local Equilibrium in Stationary States by Molecular-Dynamics," *Physical Review A,* vol. 28, pp. 3132-3133, 1983.

[24] P. L. Kapitza, "The study of heat transfer in helium II," *Journal of Physics-Ussr,* vol. 4, pp. 181-210, 1941.

[25] G. L. Pollack, "Kapitza Resistance," *Reviews of Modern Physics,* vol. 41, pp. 48-81, 1969.

[26] J. L. Barrat and F. Chiaruttini, "Kapitza resistance at the liquid-solid interface," *Molecular Physics,* vol. 101, pp. 1605-1610, Jun 10 2003.

[27] D. Chaudhuri, A. Chaudhuri, and S. Sengupta, "Heat conduction through a trapped solid: the effect of structural changes on the thermal conductance," *Journal of Physics-Condensed Matter,* vol. 19, p. 152201, Apr 18 2007.

[28] D. Chaudhuri and A. Dhar, "Heat conduction in a confined solid strip: Response to external strain," *Physical Review E,* vol. 74, p. 016114, Jul 2006.

[29] E. T. Swartz and R. O. Pohl, "Thermal-Boundary Resistance," *Reviews of Modern Physics,* vol. 61, pp. 605-668, Jul 1989.

[30] D. G. Cahill, W. K. Ford, K. E. Goodson, G. D. Mahan, A. Majumdar, H. J. Maris, R. Merlin, and S. R. Phillpot, "Nanoscale thermal transport," *Journal of Applied Physics,* vol. 93, pp. 793-818, Jan 15 2003.

[31] L. Xue, P. Keblinski, S. R. Phillpot, S. U. S. Choi, and J. A. Eastman, "Two regimes of thermal resistance at a liquid-solid interface," *Journal of Chemical Physics,* vol. 118, pp. 337-339, Jan 1 2003.

[32] R. S. Prasher and P. E. Phelan, "A scattering-mediated acoustic mismatch model for the prediction of thermal boundary resistance," *Journal of Heat Transfer-Transactions of the Asme,* vol. 123, pp. 105-112, Feb 2001.

[33] L. Xue, P. Keblinski, S. R. Phillpot, S. U. S. Choi, and J. A. Eastman, "Effect of liquid layering at the liquid-solid interface on thermal transport," *International Journal of Heat and Mass Transfer,* vol. 47, pp. 4277-4284, Sep 2004.

[34] R. J. Stevens and P. M. Norris, "Molecular-dynamics study of thermal boundary resistance," *Proceedings of IMECE04,* Anaheim, California USA, Nov 2004.

[35] R. J. Stevens, L. V. Zhigilei, and P. M. Norris, "Effects of temperature and disorder on thermal boundary conductance at solid-solid interfaces: Nonequilibrium molecular dynamics simulations," *International Journal of Heat and Mass Transfer,* vol. 50, pp. 3977-3989, Sep 2007.

[36] P. K. Schelling, S. R. Phillpot, and P. Keblinski, "Comparison of atomic-level simulation methods for computing thermal conductivity," *Physical Review B,* vol. 65, p. 144306, Apr 1 2002.

[37] J. W. Che, T. Cagin, and W. A. Goddard, "Thermal conductivity of carbon nanotubes," *Nanotechnology,* vol. 11, pp. 65-69, Jun 2000.

[38] K. V. Tretiakov and S. Scandolo, "Thermal conductivity of solid argon from molecular dynamics simulations," *Journal of Chemical Physics,* vol. 120, pp. 3765-3769, Feb 22 2004.

[39] P. Borgelt, C. Hoheisel, and G. Stell, "Exact Molecular-Dynamics and Kinetic-Theory Results for Thermal Transport-Coefficients of the Lennard-Jones Argon Fluid in a Wide Region of States," *Physical Review A,* vol. 42, pp. 789-794, Jul 15 1990.

[40] A. J. H. McGaughey and M. Kaviany, "Thermal conductivity decomposition and analysis using molecular dynamics simulations. Part I. Lennard-Jones argon," *International Journal of Heat and Mass Transfer,* vol. 47, pp. 1783-1798, Apr 2004.

[41] N. V. Priezjev, "Rate-dependent slip boundary conditions for simple fluids," *Physical Review E,* vol. 75, p. 051605, May 2007.

[42] S. Volz, J. B. Saulnier, M. Lallemand, B. Perrin, P. Depondt, and M. Mareschal, "Transient Fourier-law deviation by molecular dynamics in solid argon," *Physical Review B,* vol. 54, pp. 340-347, Jul 1 1996.

[43] A. Tenenbaum, G. Ciccotti, and R. Gallico, "Stationary Non-Equilibrium States by Molecular-Dynamics - Fourier Law," *Physical Review A,* vol. 25, pp. 2778-2787, 1982.

[44] P. Xu, T. Cagin, and W. A. Goddard, "Assessment of phenomenological models for viscosity of liquids based on nonequilibrium atomistic simulations of copper," *Journal of Chemical Physics,* vol. 123, p. 104506, Sep 8 2005.

[45] J. Koplik, J. R. Banavar, and J. F. Willemsen, "Molecular-Dynamics of Poiseuille Flow and Moving Contact Lines," *Physical Review Letters,* vol. 60, pp. 1282-1285, Mar 28 1988.

VITA

Name:	Bo Hung Kim
Address:	101-905, SeonHak Apt, ChimSan 3 Dong, BukGu, DaeGu, DaeGu, 702-053 Republic of Korea
Email Address:	bohungk@gmail.com
Education:	B.A., Mechanical Engineering, Yonsei University, 2002 M.S., Mechanical Engineering, Texas A&M University, 2006 Ph.D., Mechanical Engineering, Texas A&M University, 2009